การเตรียมเกล็ดประกายมุกจากเปลือกหอยแมลงภู่

นางสาวฐิลักษกรฐ์ จิรพิสิฐกุล

วิทยานิพนธ์นี้เป็นส่วนหนึ่งของการศึกษาตามหลักสูตรปริญญาวิทยาศาสตรมหาบัณฑิต
สาขาวิชาเคมี ภาควิชาเคมี
คณะวิทยาศาสตร์ จุฬาลงกรณ์มหาวิทยาลัย
ปีการศึกษา 2555
ลิขสิทธิ์ของจุฬาลงกรณ์มหาวิทยาลัย

PREPARATION OF PEARLESCENT FLAKES FROM GREEN MUSSEL SHELLS

Miss Thiluksakorn Jirapisitkul

A Thesis Submitted in Partial Fulfillment of the Requirements
for the Degree of Master of Science Program in Chemistry
Department of Chemistry
Faculty of Science
Chulalongkorn University
Academic Year 2012

Thesis Title   PREPARATION OF PEARLESCENT FLAKES FROM
                      GREEN MUSSEL SHELLS

By   Miss Thiluksakorn Jirapisitkul

Field of Study   Chemistry

Thesis Advisor   Associate Professor Sanong Ekgasit, Ph.D.

Thesis Co-advisor   Associate Professor Chuchaat Thammacharoen

_____

       Accepted by the Faculty of Science, Chulalongkorn University in Partial
Fulfillment of the Requirements for the Master's Degree

       …………………………………………..Dean of the Faculty of Science

       (Professor Supot Hannongbua, Dr. rer. nat.)

THESIS COMMITTEE

       ….………………………………………. Chairman

       (Assistance Professor Preecha Lertpratchya, Ph.D.)

       …………………………………….………… Thesis Advisor

       (Associate Professor Sanong Ekgasit, Ph.D.)

       ………………………………………….. Thesis Co-advisor

       (Associate Professor Chuchaat Thammacharoen)

       ………………………………………….. Examiner

       (Kanet Wongravee, Ph.D.)

       ………………………………………….. Examiner

       (Boonrat Lohwongwatana, Ph.D.)

       ………………………………………….. External Examiner

       (Associate Professor Chinapong Kritayakornupong, Dr. rer. nat.)

ฐิลักษกรฐ์ จิรพิสิฐกุล: การเตรียมเกล็ดประกายมุกจากเปลือกหอยแมลงภู่.
(PREPARATION OF PEARLESCENT FLAKES FROM GREEN MUSSEL
SHELLS) อ. ที่ปรึกษาวิทยานิพนธ์หลัก: รศ.ดร. สนอง เอกสิทธิ์, อ.ที่ปรึกษาวิทยานิพนธ์
ร่วม: รศ.ชูชาติ ธรรมเจริญ, 55 หน้า.

สีประกายมุกแสดงสีที่หลากหลาย ซึ่งเปลี่ยนไปตามมุมในการมองแต่ละครั้ง เปลือก
หอยแมลงภู่แสดงปรากฏการณ์ประกายมุกออกมาอย่างชัดเจน และสามารถแปรรูปให้เป็นเกล็ดที่มี
ความเงาและแวววาว ขยะเปลือกหอยแมลงภู่จากอุตสาหกรรมอาหารทะเลมีจำนวนมหาศาลและ
ก่อให้เกิดมลพิษทางสิ่งแวดล้อม งานวิจัยนี้เป็นการลดปริมาณและเพิ่มมูลค่าให้กับขยะเปลือกหอย
โครงสร้างของเปลือกหอยนี้มีโครงสร้างคล้ายอิฐและปูน ที่ประกอบด้วยแคลเซียมคาร์บอเนตอัญรูป
อะราโกไนต์ และโปรตีน การเตรียมเกล็ดประกายมุกจากเปลือกหอยแมลงภู่ทำได้โดยการสลายโปรตีน
ด้วยกระบวนการทางเคมีและความร้อน ศึกษาเอกลักษณ์ทางโมเลกุลและโครงสร้างของเปลือก
หอยแมลงภู่และเกล็ดประกายมุกด้วย เทคนิคกล้องจุลทรรศน์ เทคนิคกล้องจุลทรรศน์อิเล็กตรอนแบบ
ส่องกราด เทคนิคอินฟราเรดสเปกโทรสโกปี เทคนิครามานสเปกโทรสโกปี และ เทคนิคการวิเคราะห์
การสูญเสียน้ำหนักโดยใช้ความร้อน ขนาดของเกล็ดประกายมุกอยู่ในช่วง 5 – 200 ไมโครเมตร และมี
อัตราส่วนความหนาอยู่ที่ 10 แคลเซียมคาร์บอเนตอัญรูปอะราโกไนต์ในแต่ละชั้นมีความกว้าง 5
ไมโครเมตร และความหนา 200 – 500 นาโนเมตร ทั้งนี้ยังคงมีโปรตีนปริมาณเล็กน้อย (ประมาณ 2.2%
ของน้ำหนัก) เหลืออยู่ในแผ่นอะราโกไนต์ซึ่งไม่สามารถกำจัดออกได้ สีประกายมุกของเกล็ดประกาย
มุกที่เตรียมได้นี้มีสีขุ่นมัว ถ้าไม่ได้รับการปรับปรุงด้วยสารละลายกรดไฮโดรคลอริก เพื่อกำจัดฝุ่น
แคลเซียมคาร์บอเนตส่วนเกินออกจากผิวหน้าของเกล็ดประกายมุก เกล็ดประกายมุกที่มีสีประกายมุก
ชัดเจนนั้นมีความแวววาวสวยงาม และเหมาะสำหรับการนำไปใช้ในเครื่องสำอาง สีเคลือบรถยนต์ และ
วัสดุตกแต่งต่างๆ

ภาควิชา	เคมี	ลายมือชื่อนิสิต
สาขาวิชา	เคมี	ลายมือชื่ออ.ที่ปรึกษาวิทยานิพนธ์หลัก
ปีการศึกษา	2555	ลายมือชื่ออ.ที่ปรึกษาวิทยานิพนธ์ร่วม

5471959323 : MAJOR CHEMISTRY

KEYWORDS : PEARLESCENT COLOR / GREEN MUSSEL SHELL / ARAGONITE CALCIUM CARBONATE

THILUKSAKORN JIRAPISITKUL: PREPARATION OF PEARLESCENT FLAKES FROM GREEN MUSSEL SHELLS. THESIS ADVISOR: ASSOC. PROF. SANONG EKGASIT, Ph.D., THESIS CO-ADVISOR: ASSOC.PROF. CHUCHAAT THAMMACHAROEN, 55 pp.

Pearlescent color is dynamic multiple colors, which change with viewing angles. Green mussel shells show clear pearlescent phenomena and can be transformed into shiny lustrous flakes. Wasted green mussel shells from seafood industries are plenty and causing severe environmental pollution. This research reduces the amount of waste and adds value to wasted shells. The structure of this shell is a brick-and-mortar like structure consisting of aragonite calcium carbonate and protein. The preparation of pearlescent flakes from the green mussel shell is achieved via protein removal process using chemical and thermal treatments. Molecular/strutural characteristics of green mussel shells and pearlescent flakes are studied using optical microscopy, scanning electron microscopy, infrared spectroscopy, Raman spectroscopy, and thermal gravimetric analysis. The sizes of pearlescent flakes are in the range of $5 - 200$ μm with the aspect ratio of 10. The aragonite calcium carbonate in each layer is 5 μm in width and $200 - 500$ nm in thickness. There is also a slight amount of protein (~2.2 wt%) inside the aragonite tiles that cannot be removed. The pearlescent color of the prepared pearlescent flakes is dull unless the flakes are treated with hydrochloric acid in order to remove the residual calcium carbonate dust on their surface. Clean pearlescent flakes are beautiful glittering and suitable for uses in cosmetics, automotive paints, and decorative items.

Department	Chemistry	Student's Signature	
Field of Study	Chemistry	Advisor's Signature	
Academic Year	2012	Co-Advisor's Signature	

ACKNOWLEDGEMENTS

I would like to express my sincere gratitude to Associate Professor Dr. Sanong Ekgasit and Associate Professor Chuchaat Thammacharoen for wholeheartedly provide the useful guidance, understanding, training and teaching the theoretical background and technical skills during my research.

I would like to thank Assistant Professor Dr. Preecha Lertpratchya, Dr. Kanet Wongravee, Dr. Boonrat Lohwongwatana, and Associate Professor Dr. Chinapong Kritayakornupong for usefully substantial suggestions as the thesis committee.

Warmest thanks to my colleagues and organization: Sensor Research Unit, Department of Chemistry, Faculty of Science, Chulalongkorn University, and all good friends for the suggestions and spiritual supports throughout this research.

I would also especially like to thank the partial financial supports in my research: Chulalongkorn University Graduate Scholarship to Commemorate the 72nd Anniversary of His Majesty King Bhumibol Adulyadej, The National Research Council of Thailand (NRCT), Center of Innovative Nanotechnology Chulalongkorn University (CIN-CU), Center of Excellence on Petrochemical and Materials Technology.

Whatever shortcomings in the thesis remain, they are the sole responsibility of the author

Above all, I am profoundly grateful to my parents and endearing family for all their loves, understanding, support, and encouragement during the whole period of my study.

CONTENTS

LIST OF FIGURES

Page

LIST OF TABLES

LIST OF ABBREVIATIONS

FT-IR	: Fourier Transform infrared
DRIFTS	: Diffuse reflectance infrared Fourier transform spectroscopy
K-M	: Kubelka-Munk
DTGS	: Deuterated triglycine sulfate
SEM	: Scanning electron microscope
TG	: Thermal gravimetric
NaOH	: Sodium hydroxide
KOH	: Potassium hydroxide
H_2O_2	: Hydrogen peroxide
$CaCO_3$	: Calcium carbonate
HCl	: Hydrochloric acid
DI	: Deionized
CO_3^{2-}	: Carbonate ion
CCD	: Charge Couple Device
mm	: Millimeter (10^{-3} m)
μm	: Micrometer (10^{-6} m)
nm	: Nanometer (10^{-9} m)
cm^{-1}	: Wavenumber
kV	: Kilovolt (10^3 V)
M	: Molar
°C	: Celsius
h	: Hour
L^{-1}	: Per lite
kg^{-1}	: Per kilogram
g^{-1}	: Per gram
wt%	: Percent by weight
mg	: Milligram (10^{-3} g)

μg   : Microgram (10^{-6} g)

ng   : Nanogram (10^{-9} g)

pg   : Picogram (10^{-12} g)

Cd   : Cadmium

Ge   : Germanium

KBr   : Potassium bromide

R   : Reflectance

s   : Scattering coefficient

c   : Concentration

υ_0 : Frequency

ΔE   : Energy different

λ   : Wavelenght

D   : Diameter

n.a.   : Numerical aperture

e.g.   : For example

CHAPTER I

INTRODUCTION

1.1   Background

Pearlescent color appears in natural material like mollusk's shell, fish scale, bird feathers, and the bodies of some insects. Pearlescent phenomena are the interference of multilayer with different reflective index, suitable thickness of each layer, and smooth surface. Generally, commercial pearlescent pigments are synthesized by coating thin polymer films, glass flakes, and mica with metal or metal oxide. Nevertheless, these pigment productions need sophisticated equipment and considerable budgets.

Since 2009, the annual fishery and shellfish of Thailand production have reached 324,300 tons [1]. Statistically, Thailand ranks in the top five among the countries in the world that produce and export green mussels. Considering this huge production together with the fact that 70 percent of green mussels' total weight belongs to their shells [2], a problem regarding the management of wasted mussel shells rises. These shells are mostly eliminated by landfills; however, this method requires substantial investment and space. Alternatively, wasted shells are used as a raw material in chalk and metal absorber industry but the products have low values and the recycling processes require high energy consumption.

Shells of green mussels have aragonite calcium carbonate structures which contribute to pearlescent phenomena. Through a series of appropriate processes, these shells can be transformed into pearlescent pigments. So, it is the aim of this research to develop a process to transform wasted green mussel shells into high added-value pearlescent pigments that are light, glittery and of use in the cosmetic industry.

We are very proud to apply the knowledge of science that does not stay on the shelves anymore; it becomes a major role in our way of life. For now, as Thai citizen, we

are very happy as well as appreciate for the know-how producing by Sensor Research Unit, SRU, Department of Chemistry, Faculty of Science, Chulalongkorn University, as a part of the contribution in promoting the prosperity of the Thai economy.

1.2   Literatures Review

Calcium carbonate exists in 3 forms: calcite, aragonite, and vaterite. A normal and the most stable form of calcium carbonate is a calcite which has trigonal structure [3]. On the contrary, aragonite calcium carbonate is orthorhombic and relatively unstable in an environment but it is a major component found in aquatic animal shells such as shrimp shells, crab shells, and mollusk shells [4]. Vaterite calcium carbonate is hexagonal; it is unstable and rarely seen.

The main compositions of mollusk shells are calcium carbonate and an organic binder. The organic binder forms thin layers (20 – 50 nm) adjoining calcium carbonate layers. This binder takes up to 5 percent of the total weight while the rest is calcium carbonate. Nacreous structure is the innermost furrow of the shell, always aragonitic in nature, exclusive to Mollusca, found in bivalves, Gastropods and in the septal chambers of Cephalopod Nautilus. But it is apparently absent from Scaphopoda and Polyplacophora shells. In Gastropoda, nacre is of columnar type, comprised of small crystalline units, ''stacked-up'' in pyramids. The typical ''brick-wall'' arrangement founds in shells of Cephalopoda and Bivalvia [5]. Nacreous of green mussel shell, *Perna viridis*, is aragonite platelet which is approximately 2.6 mm in diameter and 0.45 mm thickness [6].

Pearlescent color is promoted by diffraction caused by the reflection grating structure of the shell. Pearlescent color is produced by an overlap of the light from several orders of diffraction. The strength of the pearlescent color depends on the groove density and the surface quality. A shell with high groove density and with a smooth and

even surface can produce a strong interference color [7]. Many shells show pearlescent color especially pearl oyster and green mussel shell.

A commercial pearlescent pigment can be synthesized by coating substrates such as glass flake, mica flake, Al_2O_3 flake, SiO_2 flake, and TiO_2 flake with metal oxide. The coating materials are metal oxides or chemicals that have a reflective index more than 1.8 including silicon oxide (SiO_2), aluminium oxide (Al_2O_3), calcium oxide (CaO), sodium oxide (Na_2O), boron oxide (B_2O_3), titanium oxide (TiO_2), iron oxide (Fe_2O_3 or Fe_3O_4), and zirconium oxide (ZrO_2). Coating can be done in either monolayer or multilayer fashion. For example, a monolayer of 65 - 75 wt% SiO_2, 0 - 5 wt% Al_2O_3, 5 - 12 wt% CaO, 8 - 15 wt% Na_2O, and 0 - 5 wt% TiO_2 can be coated onto glass flakes or a bilayer of iron oxide as a first layer with a second layer of TiO_2, Fe_2O_3, ZrO_2, SnO_2, Cr_2O_3, $BiOCl$, or ZnO can be coated onto mica substrate, producing multi-colored lustrous pearlescent pigment [8 - 12].

1.3   The objectives of this research

The objectives of this research are developed the chemical and thermal procedure in order to prepare pearlescent flakes from wasted green mussel shell and characterize the optical properties and molecular characters of pearlescent flakes.

1.4   The scopes of this research

1. This research will be started on Thai green mussel shell (*Perna viridis*).

2. Only chemical and thermal treatments are involved with preparation of pearlescent flake.

3. Size selection of pearlescent flake is suitable for additive cosmetic.

4. Study physical properties and optical properties of pearlescent flake by optical microscope (OM) and scanning electron microscope (SEM)

5. Study molecular characteristics of pearlescent flake by Fourier transform infrared spectroscopy (FT-IR), Raman spectroscopy, and thermal gravimetric analysis (TGA).

1.5 The benefit of this research

1. Utilization of wasted green mussel shell from the fishing industry.

2. Making more value to the wasted green mussel shell from the food industry.

3. Getting the environmentally-friendly novel materials and processes.

4. Reduction of imported raw materials from abroad that use in cosmetics and materials.

CHAPTER II

THEORETICAL BACKGROUND

2.1   Calcium carbonate

Calcium carbonate is a common mineral which has polymorph forms. Trimorphs of calcium carbonate are calcite, vaterite, and aragonite. Calcite is one of the most common minerals on the face of the Earth, comprising about 4% by weight of the Earth's crust. It is formed in many different geological environments. The examples of natural calcite are limestone and marble. Structure of calcite is trigonal that is the most stable morphology at most temperatures and pressures and in most environments. Its luster is vitreous in crystallized varieties. Calcite is transparent to opaque and may occasionally show phosphorescence or fluorescence [3].

Vaterite is a metastable phase of calcium carbonate at ambient conditions at the surface of the earth. As it is less stable than either calcite or aragonite, vaterite has a higher solubility than either of these phases. Therefore, once vaterite is exposed to water, it converts to calcite (at low temperature) or aragonite (at high temperature: ~60 °C). Vaterite does occur naturally in mineral springs, organic tissue, gallstones, and urinary calculi. Vaterite is usually colorless, its shape is spherical, and its diameter is small, ranging from 0.05 to 5 μm [3].

Aragonite is an interesting and attractive mineral in its own right. It forms interesting habits and can have a soft pretty color. Its modes of formation and relationship to calcite are both curious and intriguing. Aragonite has an orthorhombic symmetry and is technically unstable at normal surface temperatures and pressures. It is stable at higher pressures, but not at higher temperatures such that in order to keep aragonite stable with increasing temperature, the pressure must also increase. If aragonite is heated to 400 °C, it will spontaneously convert to calcite if the pressure is not also increased. Also

metamorphism that includes high pressures and low temperatures (relatively) can form aragonite. After burial, given enough time, the aragonite will almost certainly alter to calcite [4].

Aragon, Spain is where aragonite was first discovered and from where aragonite gets its name. Aragonite also has another popular habit called *flos ferri* or "flowers of iron". This is a branching, clumpy habit that can make delicate tree, coral or worm-like formations that are most unique. A steep pyramidal habit forms clusters of sharp spiked crystals sometimes referred to as a church steeple habit. Aragonite is a constituent of many sea creatures' shell structures; a curious development since calcite is the more stable form of calcium carbonate. Most bivalve animals and corals secrete aragonite for their shells and pearls are composed of mostly aragonite. The pearlization and iridescent colors in sea shells such as abalone are made possible by several minute layers of aragonite. Other environments of formation include hot springs deposits, cavities in volcanic rocks, caves and mines [4].

2.2   Aragonite calcium carbonate in shell

Abalone shell has two layers: an outer prismatic layer (rhombohedral calcite) and an inner nacreous layer (orthorhombic aragonite). Aragonitic $CaCO_3$ constitutes the inorganic component of the nacreous ceramic/organic composite (95 wt% ceramic, 5 wt% organic material). This composite comprises stacked platelets (0.5 μm thick), arranged in a brick and mortar microstructure with an organic matrix (20–50 nm thick) interlayer that is traditionally considered as serving as glue between the single platelets. The tensile strength in the direction perpendicular to the layered structure can be explained by the presence of the mineral bridges. These bridges, having a diameter of approximately 50 nm, have a tensile strength no longer determined by the critical crack size, but by the theoretical strength. Their number is such that the tensile strength of the tiles (parallel to the tile/shell surface plane) is optimized for the tile thickness of 0.5 μm [15 - 16].
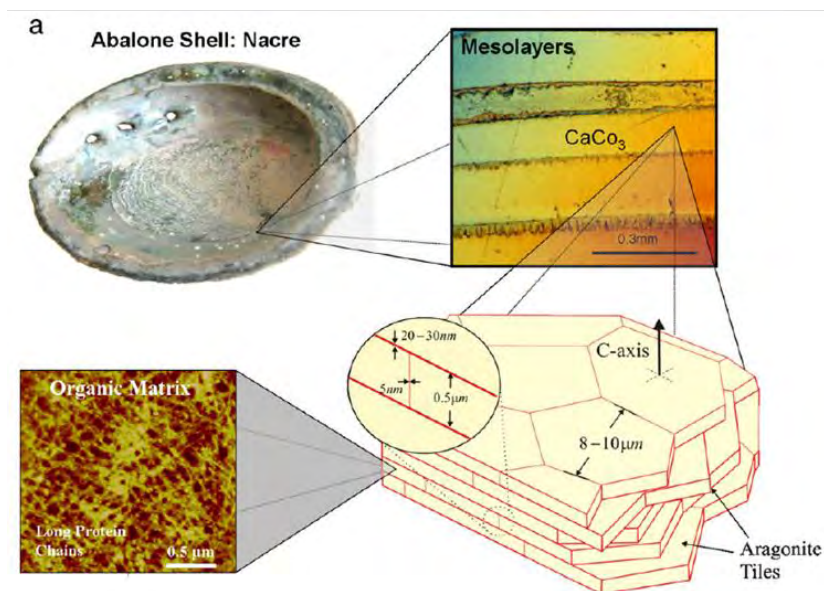
Figure 2.1 Overall view of hierarchical structure of abalone shell, showing mesolayers, mineral tiles, and tile pullout in a fracture region [15].
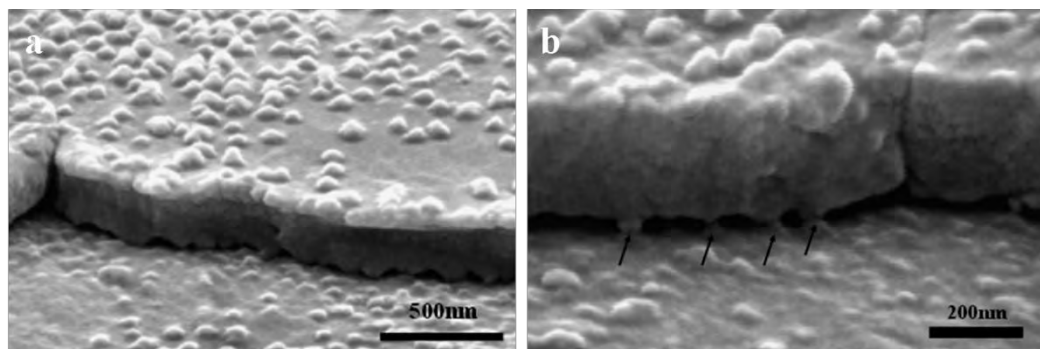
Figure 2.2 (a) Asperities (a fraction of which are remnants of mineral bridges) and (b) mineral bridges (marked by arrows) between tile layers [16].

The conch shell (*Strombus gigas*) is pure aragonite whose crossed-lamellar structure consists of criss-crossed sheets of calcium carbonate separated by protein layers, and is akin to plywood, a familiar wood/adhesive composite. The skin is a brownish

papery coating called the periostracum, below which is a thin layer of vertically oriented aragonite, a crystalline form of calcium carbonate. Crossed-lamellar layers give the shell its toughness. The basic building block of a crossed-lamellar layer is a long, thin aragonitic crystallite enclosed in a protein sheath [17].
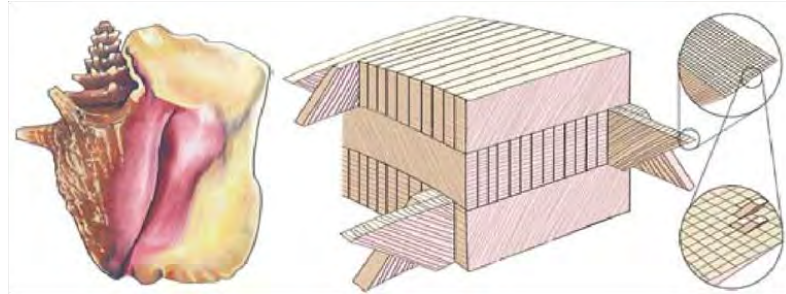
Figure 2.3   Conch shell is a layered structure. Below that layer are three crossed-lamellar layers (outer, middle and inner) in the schematic drawing of the cross section of the shell [17].

The three Gastropod and Bivalve shells are composed of crossed lamellar layers. This complex structure is composed of lamellae with alternate orientations. According to the orientation of the sections, the observed aspects seem different (Fig. 2.4). Each shell is composed of several crossed lamellar layers. The number, the orientations of these sub layers are typical of the taxa, but the basic pattern of first, second and third order lamellar seems similar [18].
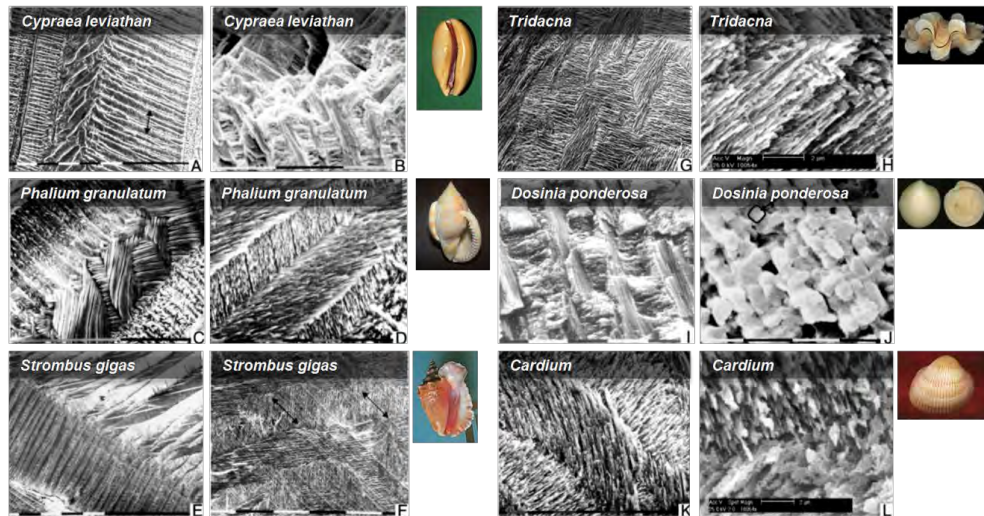
Figure 2.4 Polished and etched section and Fracture in the shell of (A) and (B) *Cypraea leviathan,* (C) and (D) *Phallium granulatum,* (E) and (F) *Strombus gigas,* (G) and (H) *Tridacna,* (I) and (J) *Dosinia ponderosa,* (K) and (L) *Cardium* [18].

The pearl oyster (*Pinctada fucat*) structure is characterized as an arrangement of continuous parallel lamellae (Fig. 2.5A), separated by sheets of interlamellar matrix. Each lamellr is composed of polygonal aragonitic tablets (Fig. 2.5B), which is sealed to each other by intertabular matrix. An aragonitic tablet seems to be a single crystal, but actually is a coherent aggregation of crystalline nanograins (about 45 nm mean size) with the same crystallographic orientation, connected by a continuous organic framework [19]. Neighbouring tablets above and below can maintain a common orientation, which again raises the issue of the transmission of mineral orientation from one row to the next. Bridges are well identified in Pinctada between successive rows in the pile, but all of those analyzed were organic and not mineral. The tablets first grow with a cylindrical shape and then turn polygonal when contacting each other. The existence of nanograins encapsulated in an organic vesicle raises the hypothesis of an aggregation-like control of the extension of the tablet by the organic template and not directly at the atomic level [20].
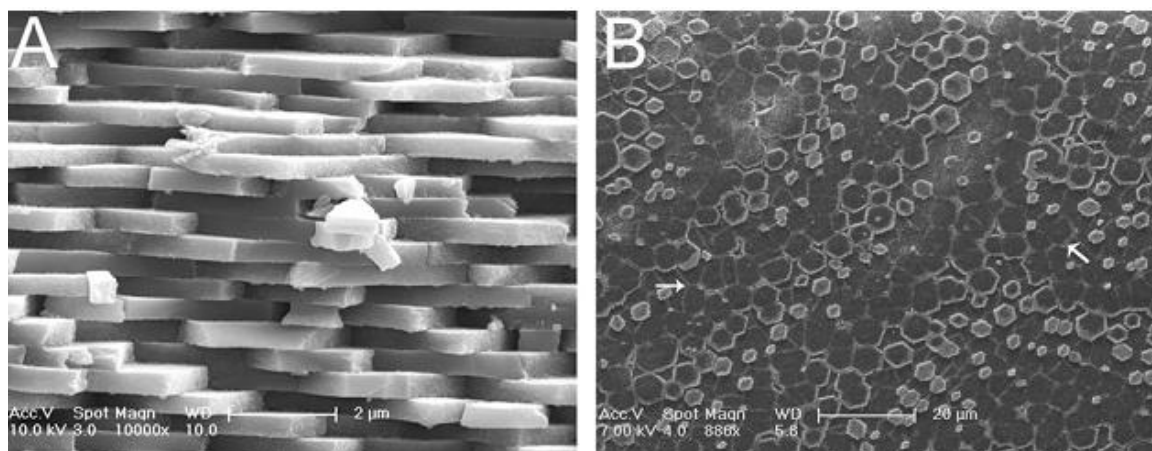
Figure 2.5 Nacre structure of *P. fucata*. (A) SEM image shows the cross-section of nacre, indicating that nacre is composed of continuous parallel lamellae. (B) Each nacre lamellae is composed of polygonal aragonitic tablets [20].

Freshwater bivalve (*H. cumingii Lea*) shell SEM observations showed that the individual growing nacre tablet exhibits typical hexagonal morphology (Fig. 2.6a). New tablets are usually nucleated at the conjunction of nacre tablets of the underlying layer and seem to grow rapidly to its full thickness which is around 500 nm. Further growth of the tablets is then accomplished by the advance of the six lateral faces until the neighboring tablets get contact. A matured tablet usually measures around 5 μm in diameter. In the present study, the lateral surfaces of the growing tablets were closely observed and revealed that they are laminated. Two examples are shown in Fig. (2.6b) and (2.6c). The nacre tablet in Fig. (2.6b) is at its early stage of the growth, while the tablets in Fig. (2.6c), which seem to grow to contact each others soon, are at their later stage of the growth. Nevertheless, they all show the laminated structure on the growing lateral surfaces, suggesting that the laminated growth pattern is a characteristic feature of the lateral growing surfaces for the nacre tablets of *H. cumingii Lea*. According to Fig. (2.6c), the average thickness of the sub-lamellae can be estimated to be less than 50 nm taken the tablet possesses a normal thickness of 500 nm and involves 10 sub-lamellae. Moreover, the sub-lamellae protrude forward in an irregularly alternative and rugged

way. It is also noticed that the remains of organic matter (white arrows in Fig. (2.6 a–c)) were not completely cleared by the wiping of cotton during sample preparation. The outmost portions of the tablets within 20–50 nm from the interlamellar organic matrix are free of the parallel stripes for both. [21]
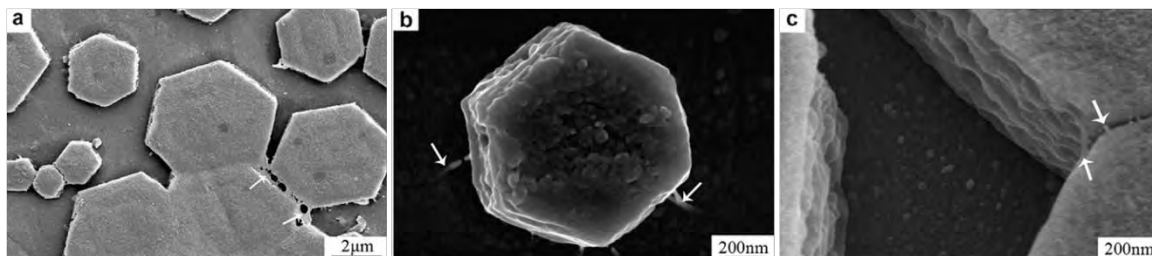
Figure 2.6   SEM images show the typical hexagonal nacre tablet: (a) the hexagonal nacre tablets at the growing stage; (b) the laminated lateral growing surfaces of the tablet at its early stage of growth; (c) the laminated lateal growing surfaces of the tablets at their late stage of growth [21].

2.3   Iridescent or pearlescent color in shell

Iridescence is a well known natural color phenomenon. It can be found in bird feathers, the bodies of some insects, and even some plants. Many shells show beautiful iridescence colors. Iridescence is mostly attributed to an interference effect caused by optical interference coatings. The iridescent color of the objects varies with changes in both the angle of incident light and the angle of observation. In mollusk's shell, the iridescent color has been attributed to a combined effect of both interferences by the layers of the nacre, and diffraction by the groove structure.
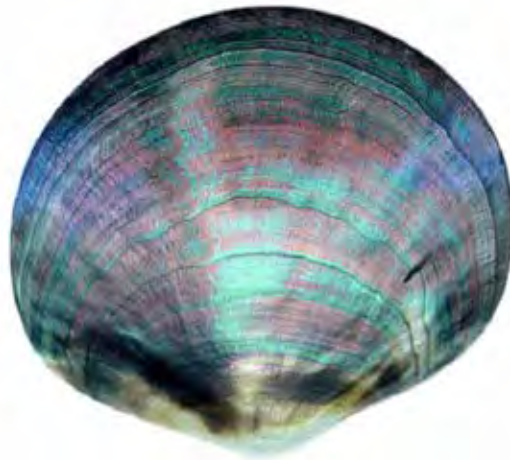
Figure 2.7 The iridescent color of a polished shell of the mollusk *Pinctada Margaritifera* [7].

The slightly curved surface structure of the shell is far from being a perfect optical quality reflection grating. The surfaces of the grooves are also slightly curved. When a light beam is incident on the surface, both surface reflection and diffraction occur. No evidence of interference was found. The light intensity at the zero order position is very intense; however, most of the light comes from the mirror surface reflection. When a light is directly incident on the shell and observed from the reflection direction, the shell does not show the iridescent color.

The intensity of the iridescent color of shells is directly related to the groove density of the diffraction grating of the shell. A shell with a diffraction grating structure at a groove density of 300 grooves/mm can show a very intense iridescent color. When the groove density is reduced to about 100 grooves/mm, the iridescent color becomes much weaker. Most shells show weaker iridescent color, and their groove densities are less than about 87 grooves/mm. The structure of each groove also affects the efficiency of diffraction produced by the shell, which in turn affects the intensity of the iridescent color. On the other hand, for a high groove density provided that their groove is smooth and evenly distributed the shell produce a strong iridescent color [7].

2.4   Green Mussel (*Perna viridis)*

Kingdom: Animalia

Phylum: Mollusca

Class: Bivalvia

Subclass: Pteriomorphia

Order: Mytiloida

Family: Mytilidae

Genus: Perna

Species: P. viridis
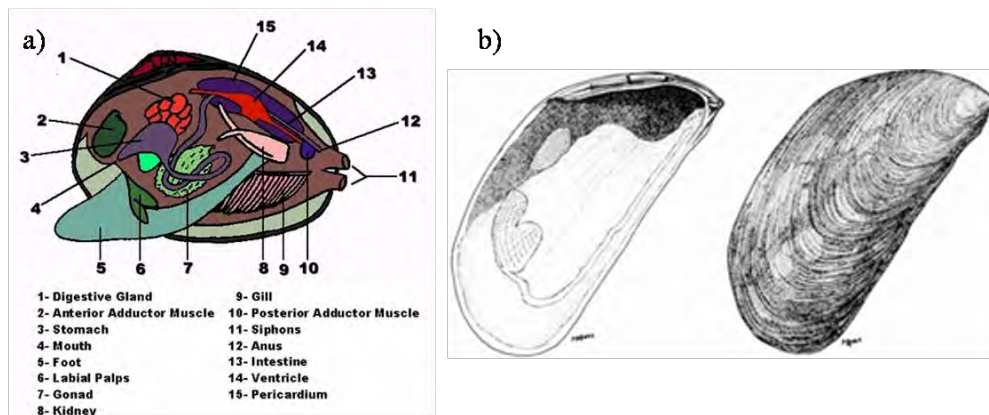
Figure 2.8   (a) Anatomy of green mussel and (b) green mussel shell.

The Asian green mussel, *Perna viridis*, is known to be native to the coastal marine waters of the Indo-Pacific region, extending from the Arabian Gulf to the southern province of Guangdong and Fujian in China and southern Japan [22 - 24]. They generally inhabit marine intertidal, subtidal and estuarine environments with high salinity. Green mussels are large, with shells typically reaching 80-100 mm in length and occasionally growing larger than 160 mm. They live for approximately three years. *P. viridis* has a

higher degree of adaptability to salinity changes and, therefore, a greater potential for aquaculture [25]. This shell is a large (> 80 mm) bivalve, with a smooth, elongate shell typical of several mytilids. It has visible concentric growth rings and a ventral margin that is distinctly concave on one side. The characteristic green coloration comes from the periostracum, the proteinaceous outer layer of the shell. It is uniformly bright green in juveniles, but dulls to brown with green margins in mature individuals. The inner surfaces of the valves are smooth and iridescent blue to bluish-green in color. A prominent, kidney-shaped retractor muscle scar is present, but the species lacks anterior adductor muscles. The lethal and sublethal effects of suspended particulate matter on the survival and physiological, behavioral and morphological features of *P. viridis* collected from Tolo Harbour, Hong Kong. They found *P. viridis* to tolerate a high level of suspended particulate matter (up to 1200 mg L^{-1}). However, there were dose-dependent effects of suspended particulate matter on the morphology of gill filaments [26].

2.4.1   Biomonitor

Green mussel is tolerated to the environment as well. So, many research uses it as biomonitor. Green mussel samples were bioindicators for organochlorine pesticides of the water quality in coastal waters along the Gulf of Thailand. The pest control chemical has produced its share of pesticide poisonings and wider environmental contamination, especially in the agricultural sector [27]. An estimation of the activities of glucose-6-phosphate dehydrogenase (G6PDH) and lactate dehydrogenase (LDH) in the adductor muscles of the mussels showed a significant, negative correlation with ambient dissolved oxygen (DO) levels [28].

Heavy metals are toxic to aquatic organisms. Copper- and mercury-exposed mussels showed increased oxygen consumption and ammonia excretion rates. The increased oxygen consumption is indicative of an increased energy requirement, while increased ammonia excretion is indicative of increased protein catabolism.

Inhibition of respiration by Cd has been attributed to mucus production because it reduces the efficiency of gaseous exchange [29 - 31].

Various antifouling biocides were surveyed in sediment and green mussels from the coastal area of Thailand. The concentrations of butyltin (MBT), dibutyltin (DBT), and tiributyltin (TBT) in sediment from Thailand were in the range of 1–293 μg kg^{-1} dry wt., 1–368 μg kg^{-1} dry wt., and 2–1246 μg kg^{-1} dry wt., respectively. The concentrations of MBT, DBT, and TBT in green mussels from Thailand were in the range of 8–20 μg kg^{-1} wet wt., 4–9 μg kg^{-1} wet wt., and 4–45 μg kg^{-1} wet wt., respectively. It is indicated that the water quality in the gulf of Thailand is good [32 - 33].

Diarrhetic Shellfish Poisoning (DSP) is a human seafood poisoning caused by eating shellfish contaminated with okadaic acid. Low concentrations of okadaic acid, 6 isomers of okadaic acid, and 5 isomers of dinophysis-toxin-l (DTX-1) were detected from green mussels from 3 sites in the Johor Strait, and Singapore, between October 1995 and December 1997. The highest concentration of any single DSP toxin detected from Singapore shellfish was 97 ng g^{-1} mussel digestive tissue (wet weight) of an isomer of DTX-l (DTX-la). The maximum concentration of okadaic acid detected was 24 ng g^{-1} digestive tissue. These concentrations are well below the generally recommended limit of consumption of DSP toxins for humans (~1 pg toxin g^{-1} digestive tissue) [34].

2.5   Optical microscopy

2.5.1   Bright Field Microscopy

In Bright field microscopy, it is able to see objects in the light path because the natural pigmentation or stains absorb light differently, or because they are thick enough to absorb a significant amount of light despite being colorless. The condenser is used to focus light on the specimen through an opening in the stage. After passing through the specimen, the light is displayed in the eye with an apparent field that is much larger than the area illuminated. A disadvantage of having to rely solely on an aperture diaphragm for contrast is that beyond an optimum point the more contrast you produce the more you

distort the image. With a small, unstained, unpigmented specimen, you are usually past optimum contrast when you begin to see the image.

2.5.2 Dark field microscopy

To view a specimen in a dark field, an opaque disc is placed underneath the condenser lens, so that only light that is scattered by objects on the slide can reach the eye (Figure 2.9). Instead of coming up through the specimen, the light is reflected by particles on the slide. Everything is visible regardless of color, usually bright white against a dark background. Pigmented objects are often seen in false colors, that is, the reflected light is of a color different than the color of the object. Better resolution can be obtained using dark field as opposed to bright field viewing. [35]
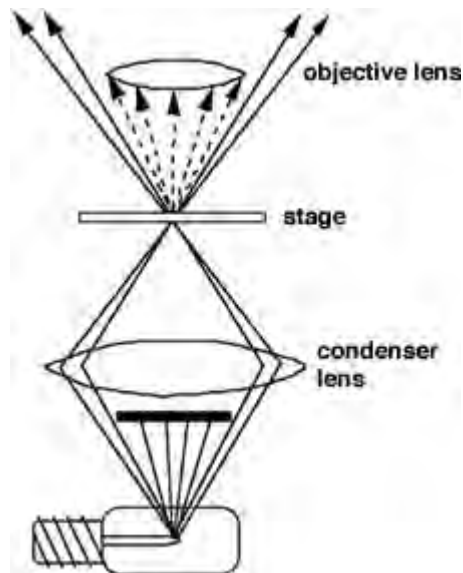
Figure 2.9 Schematic drawing optical microscope of dark field microscopy.

2.6   Infrared Spectroscopy

Infrared spectroscopy is an analytical technique for chemical identification. It is based on the fact that different chemical contains functional groups that absorb infrared light at different wavelengths dependent upon the nature of the particular functional group. Currently, there are several techniques for obtaining infrared spectra of samples. Each has its own unique advantages and disadvantages for optimizing the quality of the observed spectrum. As a result, FT-IR spectroscopy gains popularity in calcium carbonate characterization due to the direct relationship between spectral features. (i.e., chemical composition, structure and additives). There are many sampling techniques in FT-IR spectroscopy.

2.6.1 Diffuse Reflectance technique

Recently, the diffuse reflectance infrared Fourier transform spectroscopy (DRIFTS) sampling technique has gained popularity for the study of powders, solids, and species adsorbed on solids. The theory related to DRIFTS is based on incident radiation with a sample being scattering in all directions or the process which the angle of reflection is different from the angle of incidence. The scattered radiation from the sample yields the spectrum that looks very similar to the transmission spectrum of the same sample. However, the relative intensities of the absorption bands are different. The resulting spectrum can be expressed in term of Kubelka-Munk (K-M) unit. The Kubelka-Munk function is defined by the following expression (36):

$$ f(\ ) \quad \frac{(\ \ )}{} \quad \frac{k}{s} \quad \frac{.0\ ac}{s} $$

where R is the absolute reflectance of the layer, s is the scattering coefficient, c is the concentration of the sample, and k is related to the particle size and molar absorptivity of the sample by k   s/ . 0   e. The theory predicts a linear relationship between the molar

absorption coefficient and the maximum value of f( ) for each peak if the scattering coefficient, s, is a constant. The scattering coefficient is dependent on the particle size and must be constant in order to obtain quantitative results.

2.7   Raman spectroscopy

2.7.1   Theory

Raman scattering explains incident radiation of frequency (v_0). Incident radiation of frequency is considered as the stream of particles (protons) undergoing collision with molecules. If the collision was perfectly elastic, there will be any exchanges of energy between the photons and the molecule which will be exchanged of energy between the two if the collision was inelastic. A molecule can gain or lose energy which is equal to the energy difference (ΔE) between any two of its allowed states. If molecule gain energy, the scattered photons will have energy v_0 - v_m where v_m /h (Stoke scattering) and if it loses energy, the scattered photon will have energy v_0 + v_m (anti-Stokes scattering). Most of the molecules of the system, however, return to the original state from the virtual state giving the Rayleigh scatter. The vibrational spectroscopies provide key information about the molecular structure or determine the chemical identify of the sample.

2.7.2   Raman spectroscopy

Raman spectroscopy is the light scattering technique that is collected the spectrum to place a sample into the excitation beam and collects the scattered light. Raman spectroscopy has major advantages over other analytical techniques. This technique is non-destructive; it is no need to dissolve solids, press pellets, compress the sample against optical elements or otherwise alter the physical or chemical structure of a sample. Thus, Raman spectroscopy has been used extensively for analysis of physical properties such as crystallinity, phase transitions and polymorphs.

Basics of Raman spectrometer are divided into two technologies for collection of the spectra: dispersive Raman and Fourier transform Raman spectrometers. Each technique has unique advantages and is ideally suited to specific analyses.

2.7.3   Dispersive Raman spectroscopy

Dispersive Raman spectrometer is used to measure the wavelength and intensity of inelastically-scattered light which is used visible lasers, the grating and charge coupled detectors (CCD) to collect data. Dispersive Raman spectroscopy usually employs visible lasers radiation of typical laser wavelengths of 780 nm, 633 nm, 532 nm and 473 nm although others are common. One advantage of using shorter wavelength laser is the enhancement in the Raman scattering. Efficiency of Raman scattering is proportional to $1/\lambda^4$. So there is a strong enhancement as the excitation laser wavelength becomes shorter. Instrument throughput and sensitivity required the using single grating for more than one laser wavelength or more than one resolution. The grating should be specifically matched to the laser and experimental conditions.

For dispersive Raman used the CCDs commonly are silicon devices with very high sensitivity. The detecting surface of the CCD in two dimentional arrays of light sensitive elements is called pixels. Each pixel acts as the individual detector, so each dispersed wavelength is detected by a different pixel.

2.7.4   Raman Microscope

Raman spectroscopy with a microscope has the advantage on the couple of the strength with the flexibility, allowing the analysis of very small samples. The aim of microscopy is to analyze the smallest samples and distinguish the substance of interest from its surroundings as spatial resolution in microscopy. The highest spatial resolution is attained by using small pinholes or apertures somewhere in the microscope. To reach

higher resolution, it is necessary to use smaller apertures. When light passes through this smaller aperture, diffraction becomes the limiting factor. Therefore, the spatial resolution is limited by diffraction limit of laser though objective as shown by the following equation:

$$\frac{.}{\text{n.a.}}$$

where n.a, is the numerical aperture of the collection optics,   is the wavelength of the radiation and D is the diameter of collimated beam.

2.8   Scanning electron microscope

Scanning electron microscope (SEM) is widely used for observation and characterization of materials on a nanometer to micrometer scale. The signal is generated from an interaction between electron beam (e.g. secondary electron and backscattered electron) and sample. Those signals are processed and displayed as imaging signal that obtained from specific emission volumes of simple. The image signals from the secondary and backscattered electron are of great interest because these primarily show difference in the surface topography. Figure 2.10 shows electron column component of SEM.
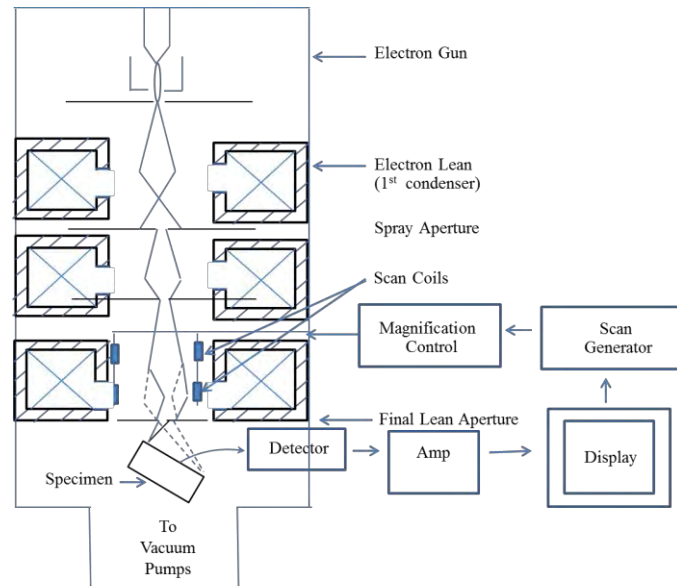
Figure 2.10   Schematic drawing SEM of the column showing electron gun, lenses the electron deflection, and electron detector.

CHAPTER III

EXPERIMENTAL   SECTION

In this research, the preparation of pearlescent flakes from wasted green mussel shell and increase pearlescent color. The pearlescent color was acquired by optical microscope. The molecular conformation of green mussel shell and pearlescent was investigated by Fourier Transform Infrared spectroscopy (FT-IR) and Raman spectroscopy. The structure of green mussel shell and pearlescent flakes was observed by Scanning electron microscopy (SEM).

3.1   Materials

1.   Green mussel shell from Samutsongkram, Gulf of Thailand.
2.   Sodium hydroxide (NaOH) was purchased from CARLO ERBA reagents, Thailand.
3.   Potassium hydroxide (KOH) was purchased from CARLO ERBA reagents, Thailand.
4.   Hydrochloric acid (HCl) was purchased from CARLO ERBA reagents, Thailand.
5.   Hydrogen peroxide (H_2O_2) was purchased from Merck KGaA, Thailand.
6.   Deionized (DI) water.

3.2   Experimental section

3.2.1   Preparation of pearlescent flakes : alkaline and thermal treatment

Pearlescent flakes were prepared by using methods as follows:

(1)   Two kinds of alkaline solution (NaOH and KOH) are used for the protein degradation.

Getting started with NaOH solution, green mussel shells were boiled in 1.0 M NaOH at 80°C for 1 h. Then the shells are washed with DI water several times and dried with room temperature.

Repeat the above procedure by using KOH instead of NaOH.

(2)   The varying concentrations of alkaline solution are as follows: 0.1 M, 0.3 M, 0.5 M, 0.7 M, and 1.0 M NaOH and/or KOH solution

(3)   Thermal treated by heating the shell in oven for 2 h and immersed them in 30 wt % H_2O_2 for 24 h. Then the shells are washed with DI water and dried.

The varying temperatures of thermal treatment are as follows: 100°C, 200°C, 300°C, 400°C, 500°C, and 600°C

Repeat step 3 by varying at different concentration:

(4)   Varying the concentrations of H_2O_2 are as follows: 10, 20, and 30 wt %

(5)   Mesh sizing of the obtained flake with 20, 40, 100, and 200 meshes, respectively.

3.2.2   Acidic treatment of pearlescent flakes

Acidic treatment of pearlescent flakes were treated by 0.5M HCl and washed with DI water and dried.

3.3   **Characterization**

3.3.1   Optical microscopy

The optical property of pearlescent flake was acquired by an optical microscope. Pearlescent flake samples were dispersed in DI water and transferred to a glass slide. All optical microscope images were taken with Axio Scope.A1 Polarized Light Microscope with AxioCam HRc camera.

3.3.1.1   Instrument
1.   Axio Scope.A1 Polarized Light Microscope
2.   AxioCam HRc

3.3.2   Fourier Transform Infrared spectroscopy (FT-IR)

The molecular conformation of green mussel shell and pearlescent was acquired by Diffuse Reflectance Infrared Fourier Transform (DRIFT). All DRIFT spectra were recorded in the frequency ranging from $500 - 4000$ cm^{-1} on Nicolet 6700 FT-IR spectrometer with a deuterated triglycine sulfate (DTGS) detector at a resolution of 4 cm^{-1}. All samples were collected at 64 co-addition times. The shell samples were ground to powder and fill in collector diffuse reflectance accessory.

3.3.2.1   Instrument
1.   Nicolet 6700 FT-IR spectrometer equipped with a deuterated triglycine sulfate (DTGS) detector.
2.   Collector Diffuse Reflectance Accessory

3.3.1.2 Default Spectral Acquisition Parameter
Nicolet 6700 FT-IR Spectrometer

Instrument Setup

Source	Standard Globar^{TM} Infrared Light Source
Detector	DTGS
Beam splitter	Ge-coated KBr

Acquisition Parameter

Spectral resolution	4 cm^{-1}
Number of scans	64 scans
Spectral format	Absorbance
Mid-infrared range	4000 – 500 cm^{-1}

3.3.3 Raman spectroscopy

The molecular conformation of green mussel shell and pearlescent was acquired by Raman spectroscopy. All Raman spectra were recorded in the frequency ranging from 150 to1500 cm^{-1} on DXR Raman spectrometer with Charge Coupled Device (CCD) detector at a resolution of 2 cm^{-1}. All samples were collected at 32 co-addition times.

3.3.3.1 Instrument
DXR Raman Microscope

3.3.3.2 Default Spectral Acquisition Parameter
DXR Raman spectrometer

Instrument Setup

Spectrometer	Visible Raman Microscope
Source	Excitation source (Laser)

Detector	CCD
Laser polarization	Parallel
Laser	532 nm
Grating	900lines/mm
Range	$1500 - 150$ cm^{-1}
Focusing objective	20X Long
Aperture size	150 μm x 150 μm
Spatial resolution	1 μm

Acquisition Parameter

Laser power	10
Spectral resolution	2 cm^{-1}
Number of scan	32 scans
Spectral format	Intensity
Spectrograph aperture	25 μm pinhole

3.3.4   Scanning electron microscope (SEM)

The structure of green mussel shell and pearlescent flakes was acquired by SEM. A shell and pearlescent flake samples were attached to a stainless steel stub through a carbon tape. Scanning electron microscopy micrographs were recorded with a JEOL 6500A (analytical electron microscope) operated at $5 - 20$ kV under high vacuum mode using a secondary electron imaging (SEI).

3.3.4.1 Instrument
JEOL 6500A Scanning electron microscope with secondary electron imaging (SEI)

Chapter IV

Results and Discussion

The shells of the green mussel and their products from each process were studied by various techniques such as Fourier transform infrared spectroscopy (FT-IR), Raman spectroscopy (Raman), optical microscope (OM), scanning electron microscopy (SEM), as well as thermal gravimetric analysis (TGA).

4.1   The shells of the green mussel (*Perma Viridis*)

The composition of the shell can be divided into 2 parts which are the organic compounds (e.g., protein, chitin, and periostracum) and calcium carbonate [37-38]. Each layer is stacked with each other as shown in Figure (4.1b) and (4.1c) for protective covering of mollusc shells [5].

At the interface of the outer and the inner shell, both layers are connected to each other by the spikes under periostracum, about 0.35 μm in diameter and 14.01 μm interval as shown in Figure (4.1d), and holes over the outer shell, 0.38 μm in diameter and 14.29 μm interval as shown in Figure (4.1e). The connection between these two layers is through physical action and can be separated easily.

The structure of the inner shell is constructed by aragonite calcium carbonate and organic compound as the linkage between layers. The shell is constructed in brick-and-mortar liked structure with 200 – 500 nm in thickness and 5 μm in size of aragonite tile as shown in Figure (4.1f) and (4.1g).
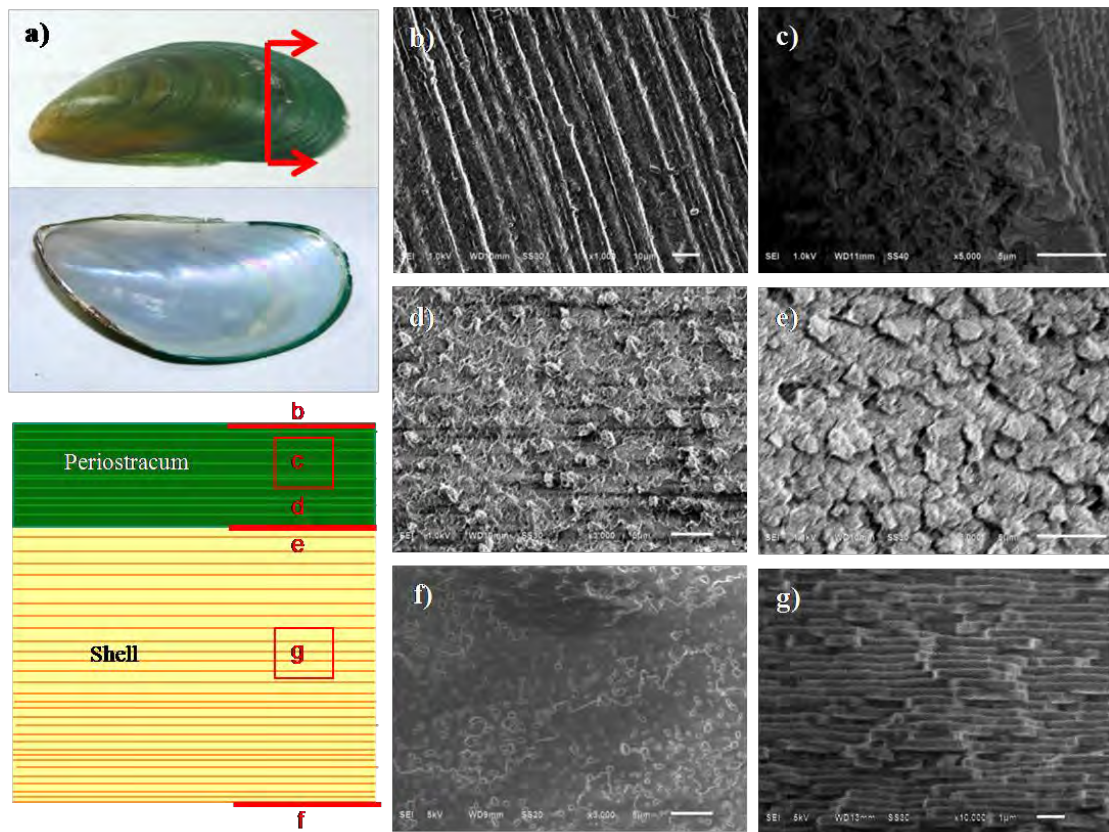
Figure 4.1 (a) Photograph of green mussel shell and SEM images of original green mussel shells (b) outer surface, (c) cross section, and (d) inner surface of the periostracum, (e) outer surface, (f) inner surface and (g) cross section of the shell and the cross section diagram of the shell.

From Figure (4.2a), FT-IR spectrums at 1083 cm^{-1} (symmetric stretching, v_1), 856 cm^{-1} (out of plane bending, v_2), 715 and 700 cm^{-1} (in of plane bending, v_4) were characteristic signals of aragonite [39 – 42] and Raman spectrums in Figure (4.2b) at 1088 (v_1), (706, 709) (v_4), 209, and 156 cm^{-1} (external lattice) were characteristic signals of aragonite [42 - 44], these evidences confirmed that calcium carbonate in the shells was aragonite.
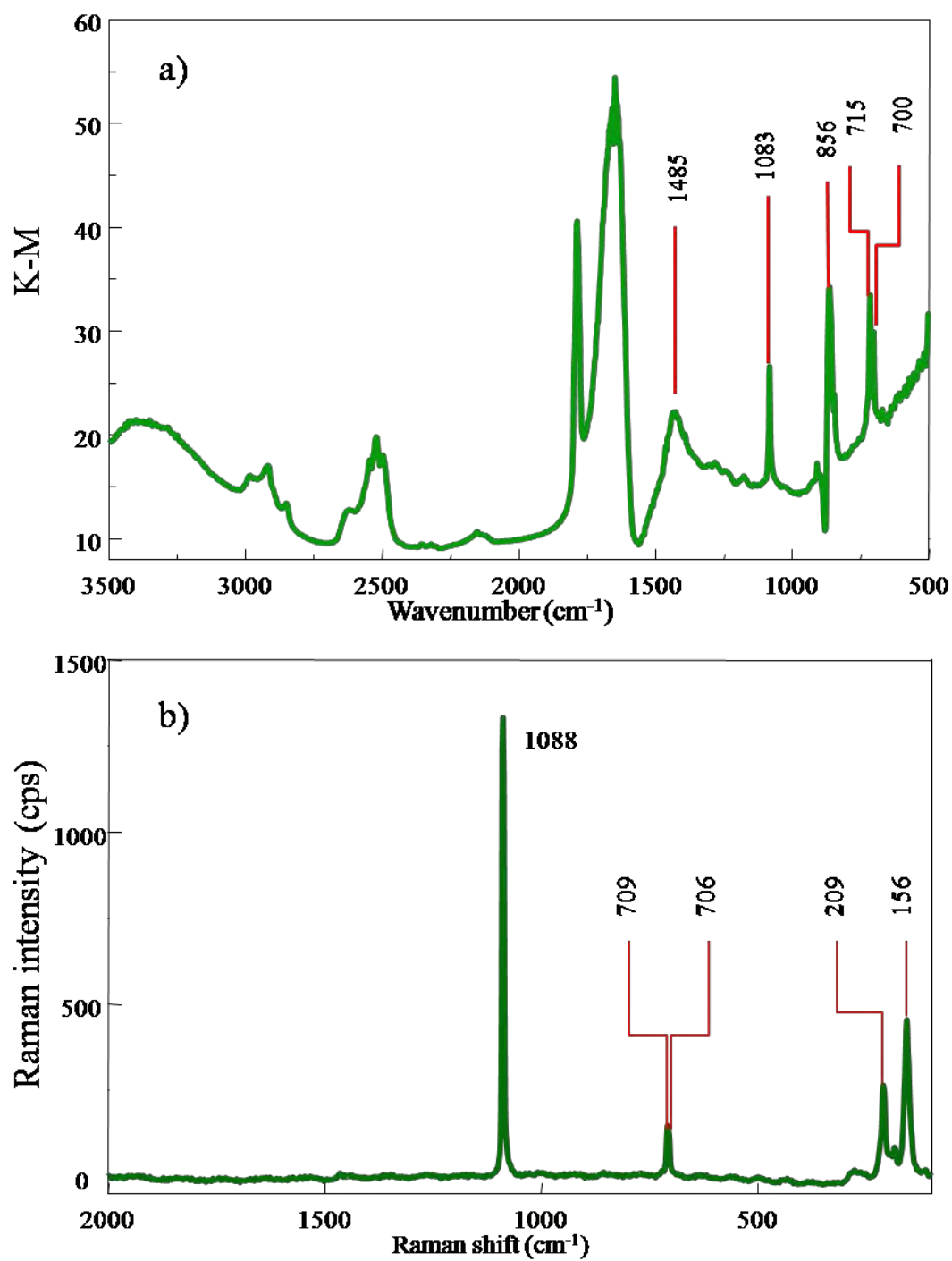
Figure 4.2   (a) FT-IR spectrum and (b) Raman spectrum of the green mussel shell.

Table 4.1   Vibration mode of CO_3^{-2} of aragonite and calcite $CaCO_3$ [42- 44].

Mode	IR		Raman	
	Aragonite	Calcite	Aragonite	Calcite
Symmetric stretching (υ_1)	1082	-	1085	1087
Out of plane bending (υ_2)	859	875	853 (very small)	847 (very small)
Asymmetric stretching (υ_3)	1485	1426	1462 (low intensity)	1437 (low intensity)
In plane bending (υ_4)	712,700	712	706, 709	715

Table 4.2   TG data of $CaCO_3$ powder (Merck), original green mussel shell with and without periostracum.

Sample	Protein content (% weight)
$CaCO_3$ powder (Merck)	-
Green mussel shell	6.9
Green mussel shell without periostracum	3.0
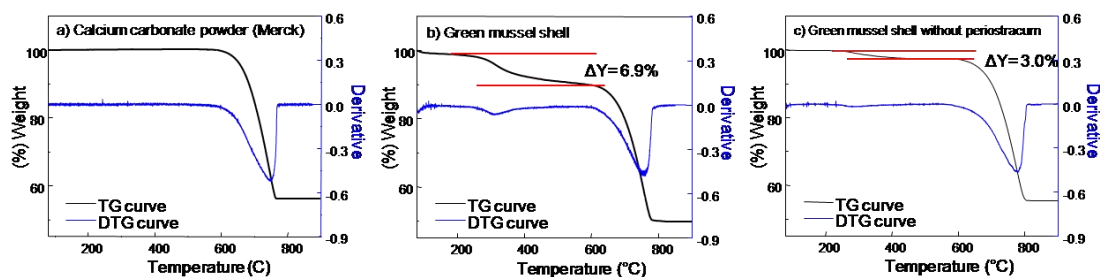
Figure 4.3   TG curves of (a) CaCO$_3$ powder (Merck) (b) original green mussel
shell with and (c) without periostracum.

From TG curves in Figure 4.3, the original mussel shell with and without
periostracum showed a %weight loss at 200 – 300 °C of 6.9 and 3.0%. Accordingly,
at 600 – 800 °C, A %weight loses was 40% that transformed calcium carbonate
(CaCO$_3$) to calcium oxide (CaO). These results confirmed that the shell consisted of
7% protein and 93% calcium carbonate.

4.2   The preparation of pearlescent flakes from green mussel shell

4.2.1   Alkaline and Thermal treatment

The elimination of protein in green mussel shells could be done by boiling the
shells in alkaline solution. Using sodium hydroxide (NaOH) and potassium hydroxide
(KOH) in 1.0 M concentration boil at 80 °C for 1 h. The result of both alkaline
solutions, they could completely digest the periostracum from the shells and the shells
remained the same shape. Moreover, the increment of luster at the inside of the shell
could be observed as shown in Figure 4.4.
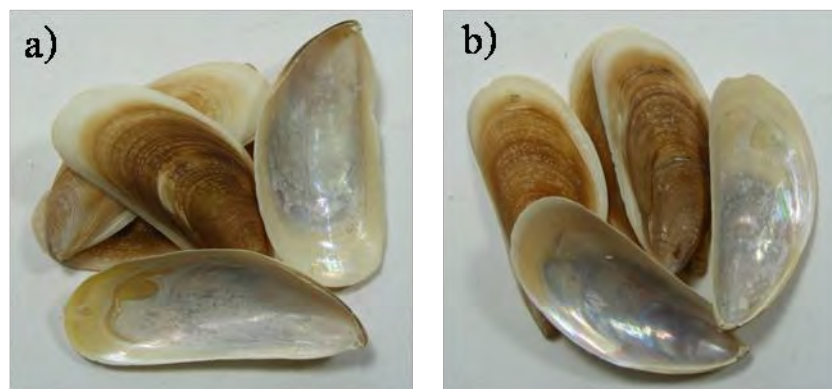
Figure 4.4   Photographs of green mussel shells after boiling in 1.0 M alkaline solution at 80 °C for 1 h (a) NaOH and (b) KOH.

The pearlescent phenomena are attributed to the scattering and refracting of light on the surface of the shell. The aragonite layer has a refractive index of 1.6 [45] and protein had a refractive index of 1.5 [46], when the incident light passes through the different refractive index medium, it scatters out in many angles and produces pearlescent phenomena. After removing the protein from the shell, the protein is replaced by air which has a refractive index of 1.0 and made the aragonite/air refractive index has more different than aragonite/protein, so, the pearlescent phenomena occurs better and more clearly.

According to the result, two types of alkaline solution produced the same outcome. So, the only KOH solution was used in subsequent steps because the product of the reaction between KOH and protein could be used as a fertilizer and it was also environmentally friendly. Boiling the shells at 80 °C for 1 h and varying the concentration of KOH solution 0.1, 0.3, 0.5, 0.7 and 1.0 M. The result at 0.1 M KOH, the periostracum still left on the shells, at 0.3 M KOH, most of the periostracum was eliminated and at 0.5 − 1.0 M KOH, all the periostracum was removed, as shown in Figure 4.5.
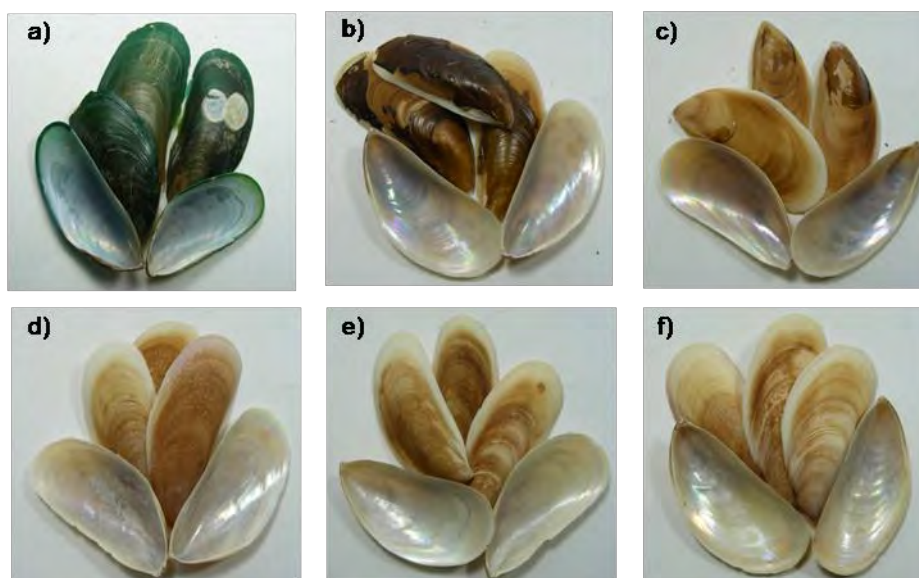
Figure 4.5   Photographs of (a) green mussel shells and shells after boiling in alkaline solutions at 80°C for 1 h, varying KOH concentration as follows: (b) 0.1, (c) 0.3, (d) 0.5, (e) 0.7, and (f) 1.0 M.

From the results, the most suitable concentration for the experiment was 0.5 M KOH, the alkaline solution could digest all the periostracum. From TG curves, protein content of alkaline treated shell was similar to shell without periostracum (3.0 wt%) (Figure 4.6). This evidence indicated that alkaline treatment did not remove interlamellar organic compound. So, this compound was eliminated by thermal treatment.
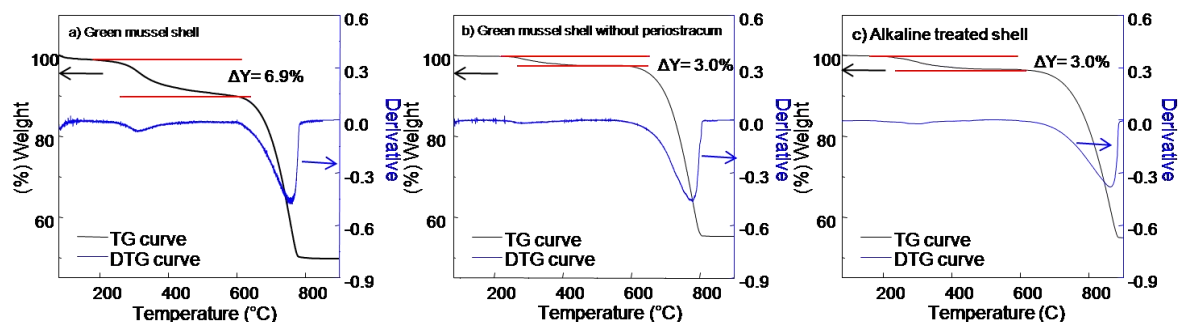
Figure 4.6   TG curves of (a) original green mussel shells, (b) no periostracum shell, and (c) Alkaline treated shell

The boiled shells were thermal treated at various temperatures, 100 °C, 200 °C, 300 °C, 400 °C, 500 °C, and 600 °C for 2 h and then, soaked in 30 wt% hydrogen peroxide solution (H_2O_2) for 24 h in order to remove the organic compound inside the shell. Figure 4.7 was final products of thermal treatment and H_2O_2 treatment. The treated shells from 100 - 300 °C were observed pearlescent phenomena. On the other hand, Treated shells from 400 – 600 °C did not show pearlescent property but had black color of burn organic compound. The treated shells from 100 °C still remained the big pieces. This may cause by the remaining protein that hold the structure together.
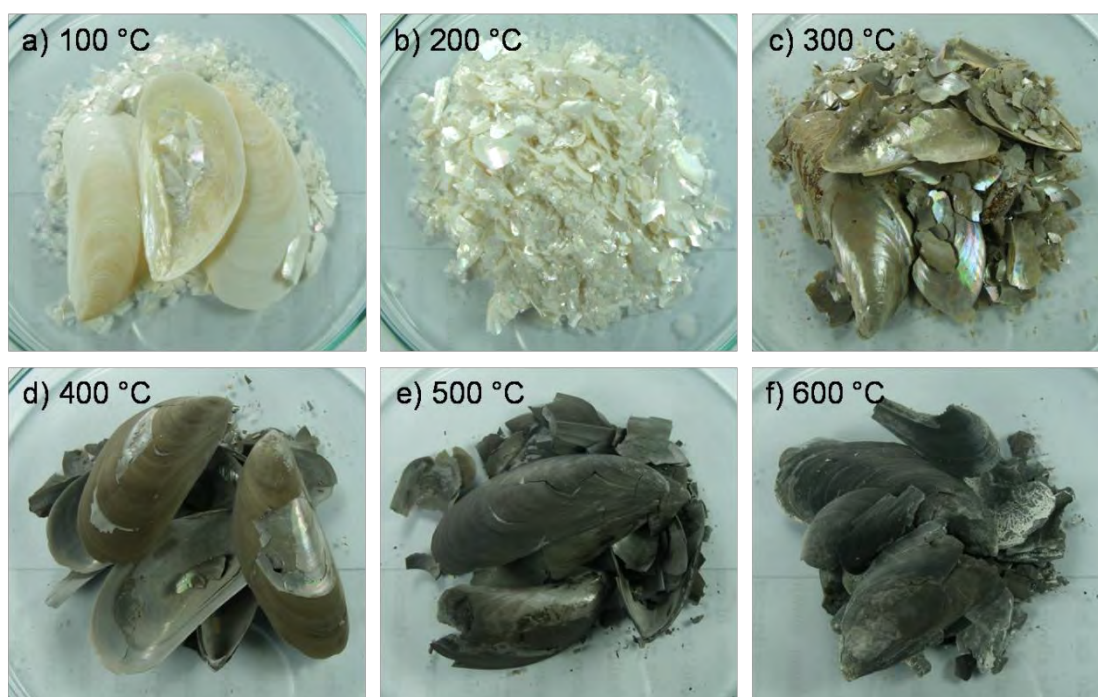
Figure 4.7   Photographs of the shells after processes, boiled in 0.5 M KOH at 80°C for 1 h, thermal treated at (a) 100 °C, (b) 200 °C, (c) 300 °C, (d) 400 °C, (e) 500 °C, and (f) 600 °C for 2 h and soaked in 30 wt% H_2O_2 for 24 h.
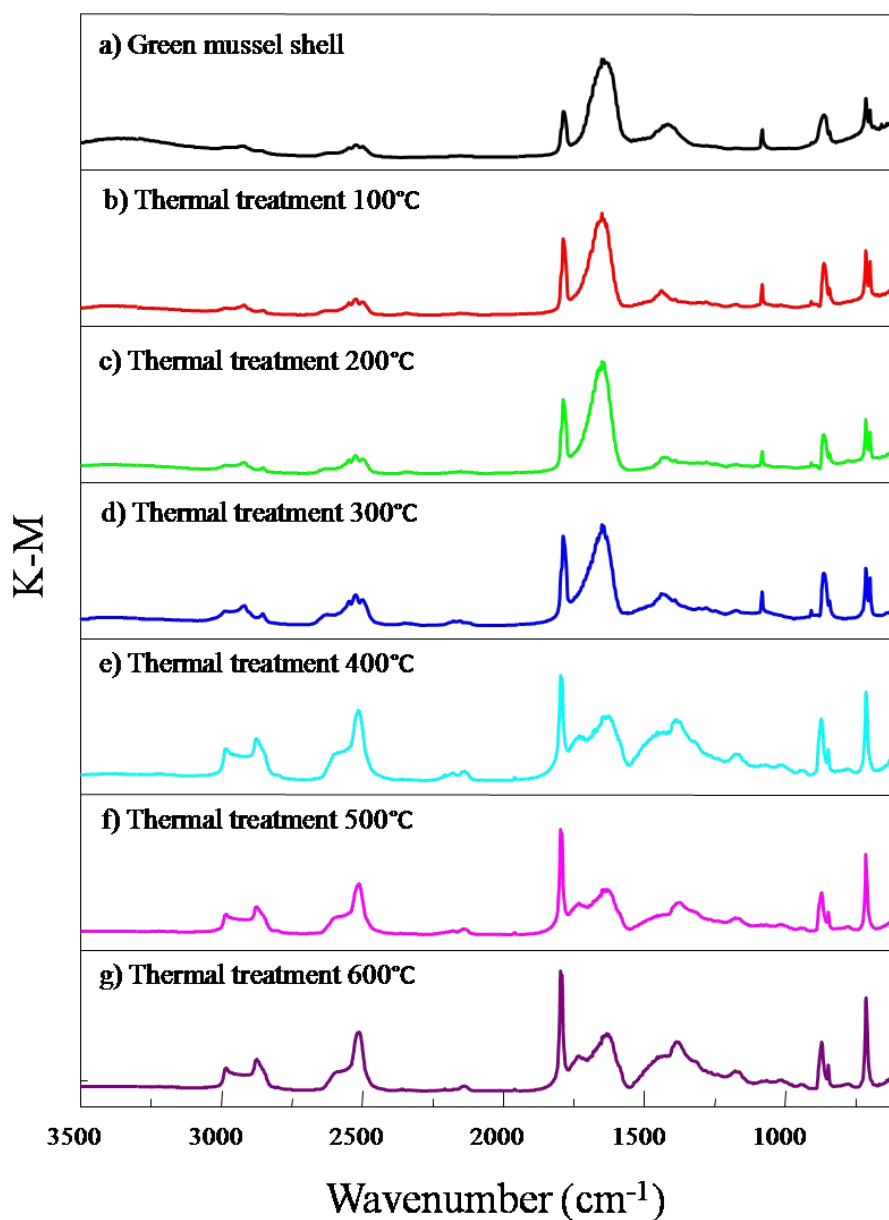
Figure 4.8 FT-IR spectrum of (a) green mussel shells and shells after boiling in 0.5 M KOH at 80 °C for 1 h, thermal treated at (b) 100 °C, (c) 200 °C, (d) 300 °C, (e) 400 °C, (f) 500 °C, and (g) 600 °C for 2 h and soaked in 30 wt% H_2O_2 for 24 h.

From FT-IR spectrum, green mussel shell after thermal treatment at 100 – 300 °C has a single band at 1083 (v_1), 856 (v_2), and double bands 715 and 700 cm^{-1} (v_4). These results indicated the signature of calcium carbonate in the aragonite form [42 -

44]. When the thermal treatment temperature increased to 400 °C, calcium carbonate in aragonite form was transformed to calcite form. As out of plane bending, v_2 was shifted to 873 cm^{-1} and double band of in plane bending, v_4 was changed to single band at 713 cm^{-1}, aragonite was completely transformed to calcite.
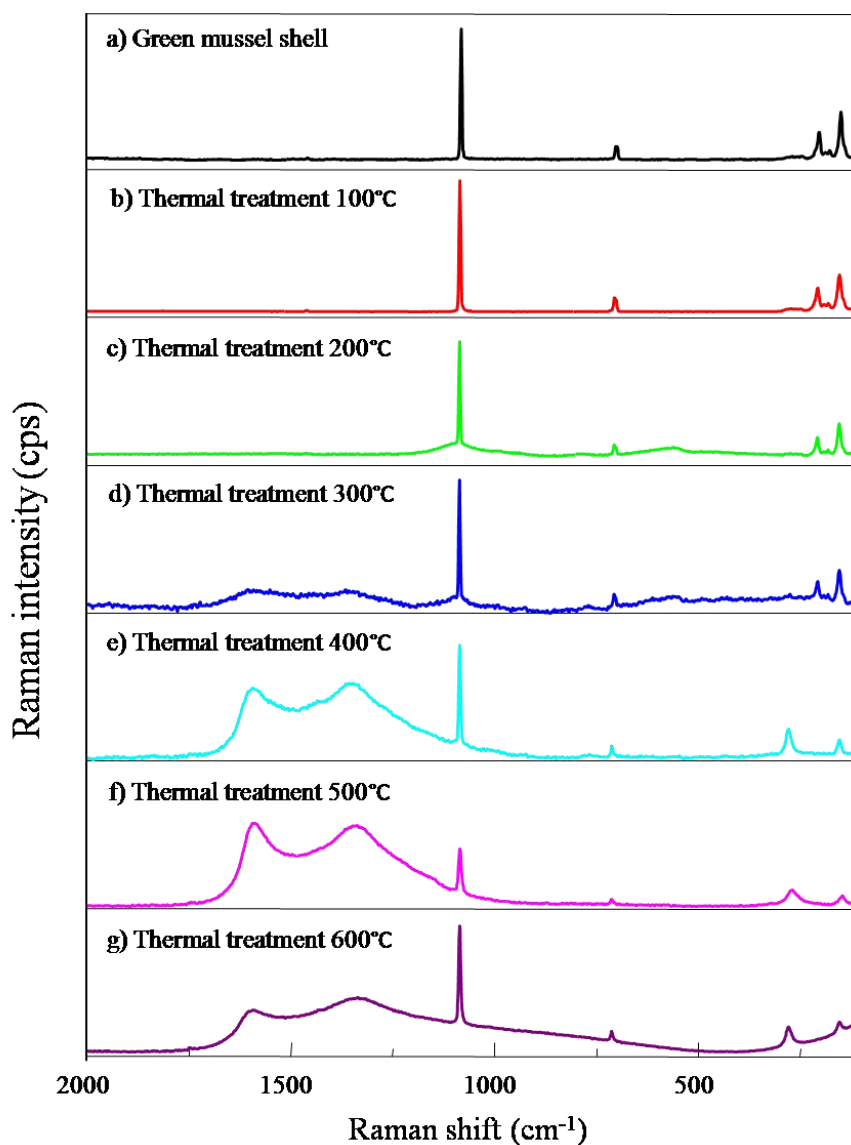

Figure 4.9   Raman spectrum of shells (a) after boiling in 0.5 M KOH at 80 °C for 1 h, and thermal treated at (b) 100°C, (c) 200°C, (d) 300°C, (e) 400°C, (f) 500°C, and (g) 600 °C for 2 h and soaked in 30 wt% H_2O_2 for 24 h.

From a Raman spectrum of each calcium carbonate after thermal treatment at various temperatures were harmonized with the FT-IR results. At 300 – 600 °C, there were 1600 and 1350 cm^{-1} signals which were disordered carbon (D band) and graphitic carbon (G band) [47], respectively. The intensity of these signals comparison with the signal at 1088 cm^{-1} (v_1) was high and even higher at 500 °C. At 600 °C the two carbon signals had lower intensity, this result might describe as the organic compound in the shell had changed into carbon dioxide (CO_2). So, the thermal treatment at 200 °C was suitable temperature where the most protein was removed and gave the white aragonite pearlescent flakes.

The shells were thermal treated at 200 °C for 2 h, soaked in 10 – 30 wt% H_2O_2 solution for 24 h, and then got the pearlescent flakes, after that, cleaned the pearlescent flakes and size the flakes selected by grating, 20, 40, 100, 200 mesh, channels per inch square, and weighed the finished flakes of each mesh.

From Figure 4.10, the higher the concentration of H_2O_2, the smaller the size of calcium carbonate were increased. At 30 wt% H_2O_2, getting the smallest calcium carbonate, so, this was the most suitable concentration to make pearlescent flakes.
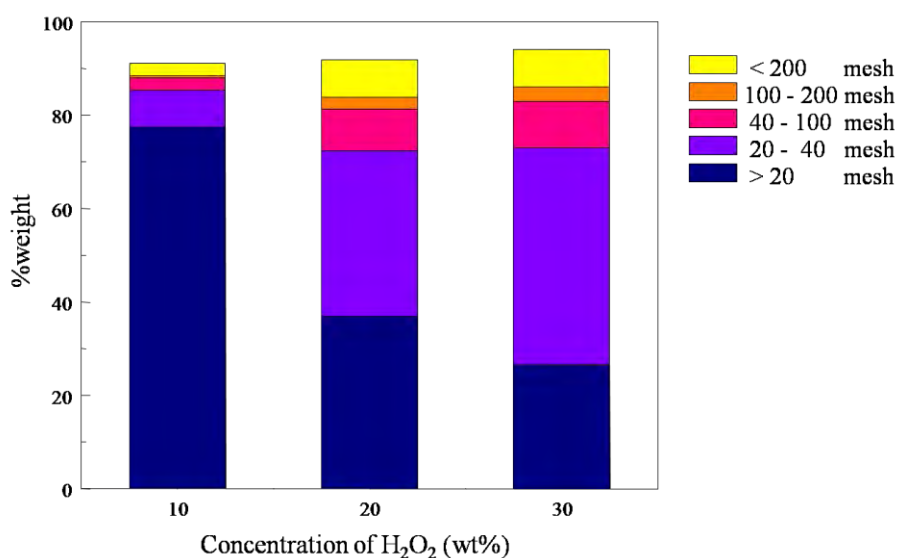
Figure 4.10 Graph % weight of size calcium carbonate at >20, 20-40, 40-100, 100-200 mesh and < 200 mesh after soaking in 10 – 30 wt% H_2O_2.

From optical microscope images of pearlescent flakes in bright field mode, the pearlescent color was clearly seen, this could be described by the scattering effect of light but in the dark field mode it seemed to be the transparent color. The flakes between 20 – 40 mesh had size around 0.5 – 1 cm, between 40 – 100 mesh had size around 200 – 500 μm, between 100 - 200 mesh had size around 50 – 100 μm and calcium carbonate powder that smaller than 200 mesh had size around 15 – 50 μm, the size of pearlescent flakes could be controlled by the size of the mesh.
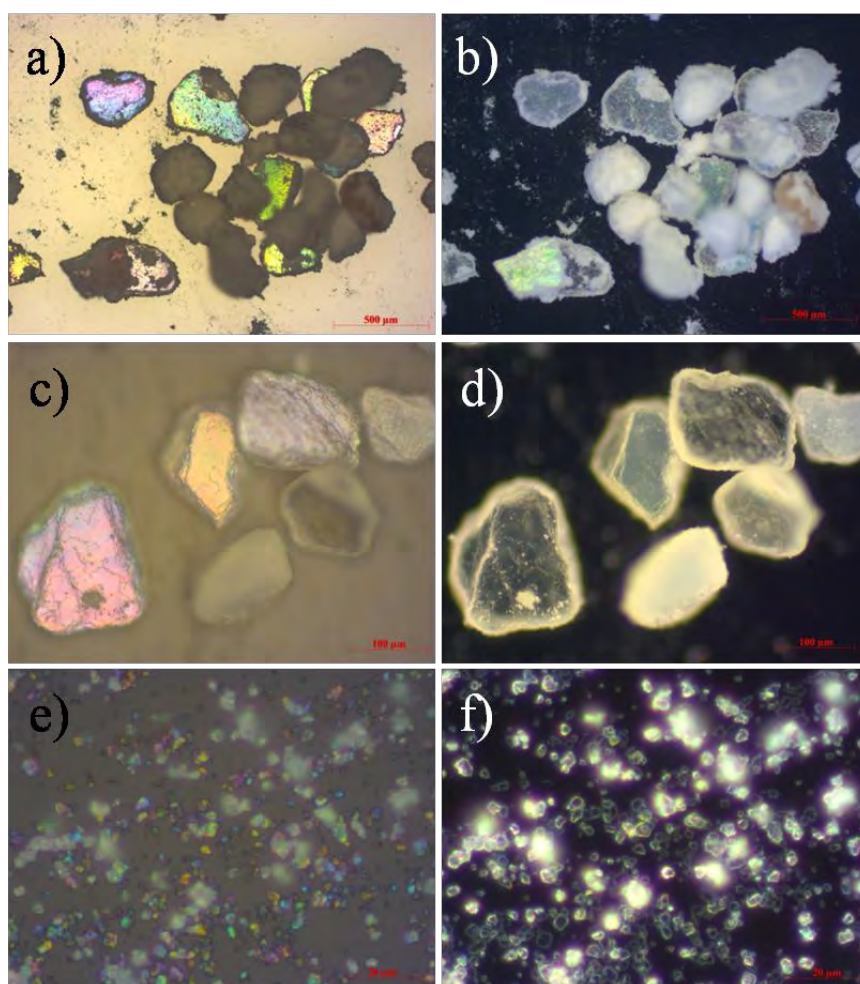
Figure 4.11   Optical microscope images of pearlescent flakes in bright field and dark field mode of (a) and (b) 200 – 500 μm, (c) and (d) 50 – 100 μm, (e) and (f) 15 – 50 μm.

SEM images of pearlescent flake shown stratified layers of aragonite calcium carbonate. The pearlescent flakes had aspect ratio of 10:1.
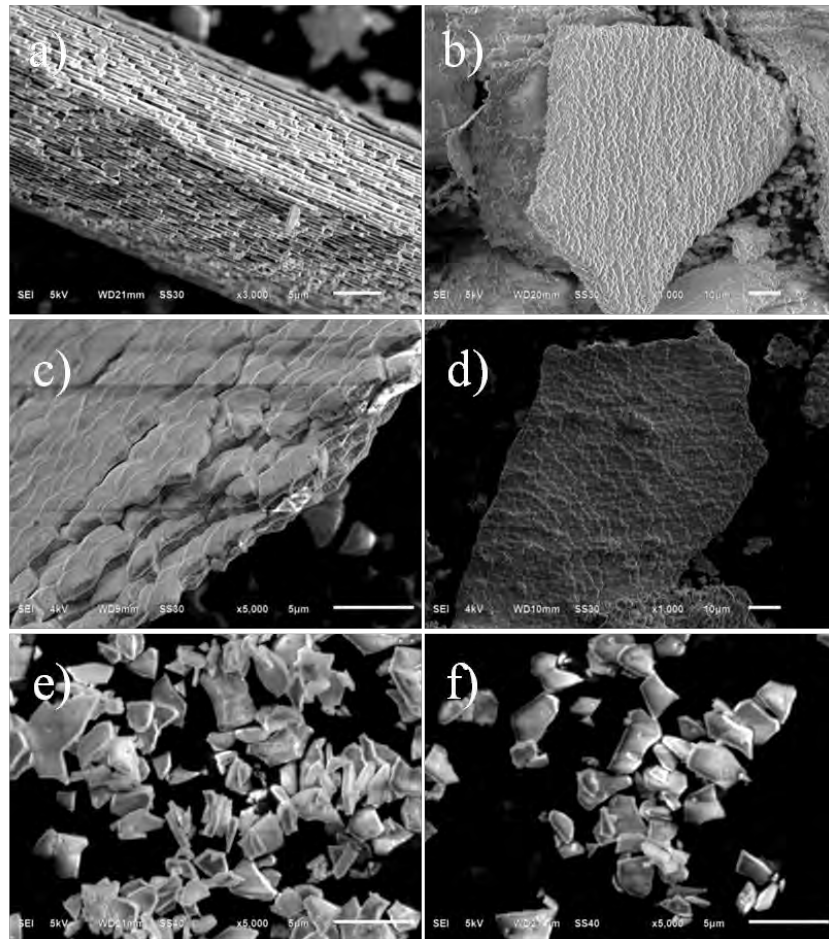
Figure 4.12   SEM images of pearlescent flakes (a) and (b) 200 – 500 μm, (c) and (d) 50 – 100 μm, (e) and (f) 15 – 50 μm.
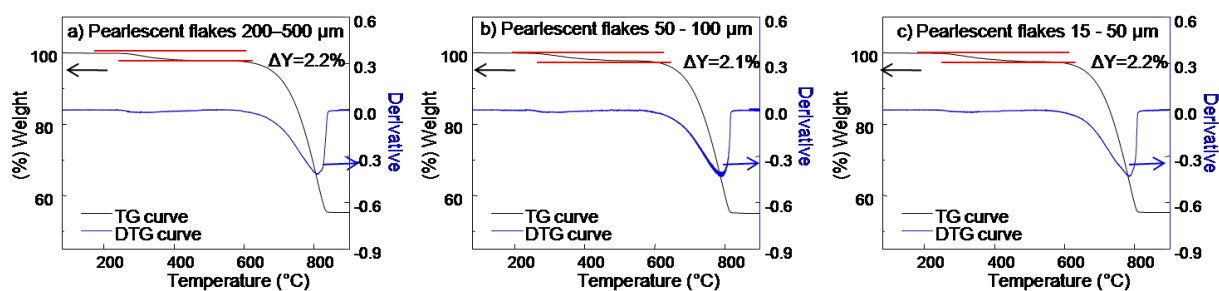
Figure 4.13   TG curves of pearlescent flakes (a) 200 – 500 µm, (b) 50 -100 µm, and

(c) 15 – 50 µm.

Table 4.3   TG information of pearlescent flakes 200 – 500 µm, 50 -100 µm, and
15 – 50 µm

Sample	Protein content (% weight)
Pearlescent flakes 200 – 500 µm	2.2
Pearlescent flakes 50 – 100 µm	2.1
Pearlescent flakes 15 – 50 µm	2.2

From TG results, shells were thermal treated at 200 °C and soaked in 30 wt% H_2O_2 for 24 h which eliminated organic compound binding in structure. The shells were dispersed to pearlescent flake, small flakes were observed pearlescent color. Every size of pearlescent flakes contained protein at 2.2 wt%―it means that this amount of protein has blended in every aragonite tile, not interlamellar aragonite layers. The evidence of this phenomenon is the TG results of pearlescent powder (15 - 50 µm), which is single plates of aragonite, that has the close amount of protein compared to those in the bigger pearlescent flakes (200 – 500 µm).

4.2.2 Thermal treatment

In alkaline and thermal treatment, there are 2 steps for digestion of organic compounds. Alkaline treatment could be removed only the periostracum. Due to thermal treatment eliminated interlamellar protein, so this treatment might be destroyed periostracum at the same time. This process was getting started with thermal treatment the shell at various temperatures and soaked in 30 wt% H_2O_2, then, characterize by FT-IR and Raman spectroscopy.

The treated shells from 100 - 300 °C were observed pearlescent phenomena. Due to treated shells from 400 – 600 °C did not show pearlescent property but had black color of burn organic compound. These evidences were similar to alkaline and thermal treatment but the periostracum removal of this process was difficult to clean.
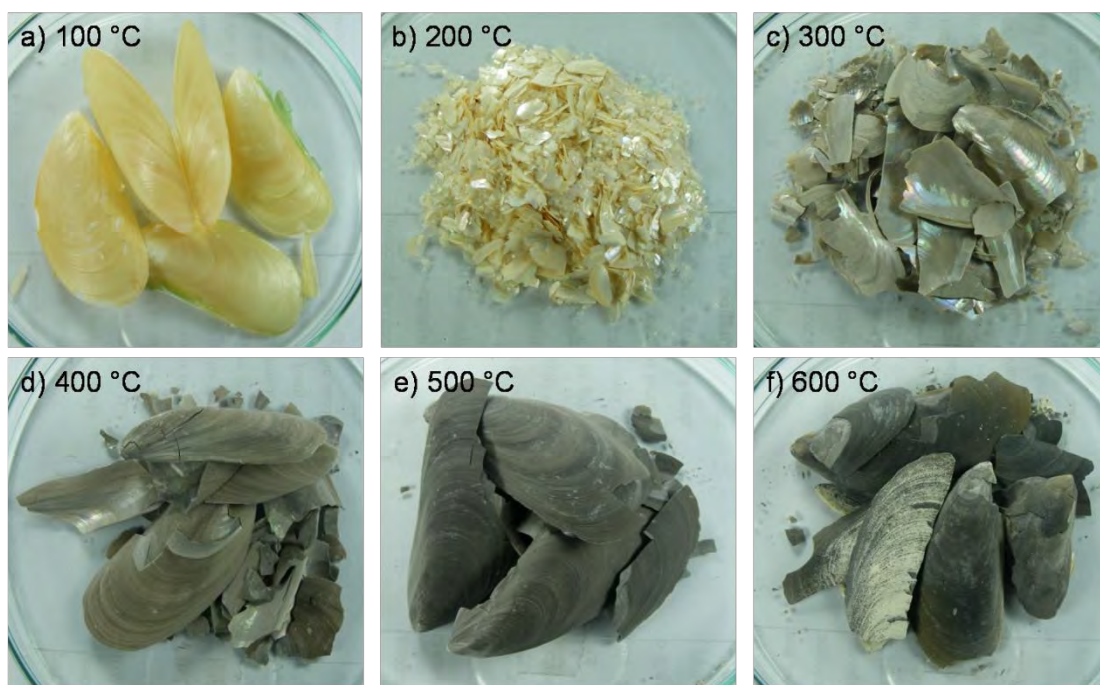
Figure 4.14   Photographs of calcined green mussel shells at (a) 100 °C, (b) 200 °C, (c) 300 °C, (d) 400 °C, (e) 500 °C, and (f) 600 °C for 2 h, and soaked in 30 wt% H_2O_2 for 24 h.

From FT-IR, the thermal treated shell at 400 °C, calcium carbonate in aragonite form was completely transformed to calcite form. As υ_2 was shifted to 873 cm^{-1} and double band of υ_4 was changed to single band at 713 cm^{-1}.
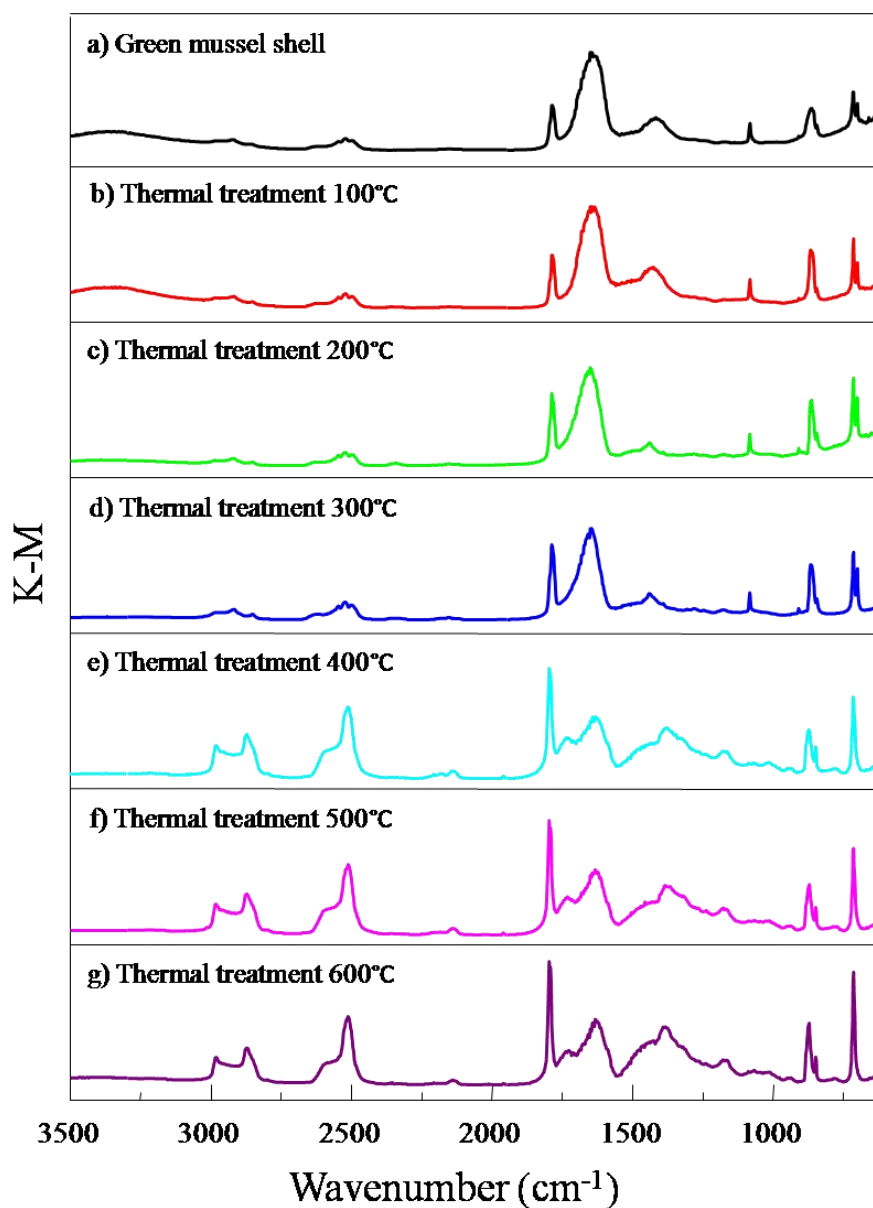
Figure 4.15 FT-IR spectrum of green mussel shells after calcined at (a) 100 °C, (b) 200 °C, (c) 300 °C, (d) 400 °C, (e) 500 °C, and (f) 600 °C for 2 h, and soaked in 30 wt% H_2O_2 for 24 h.
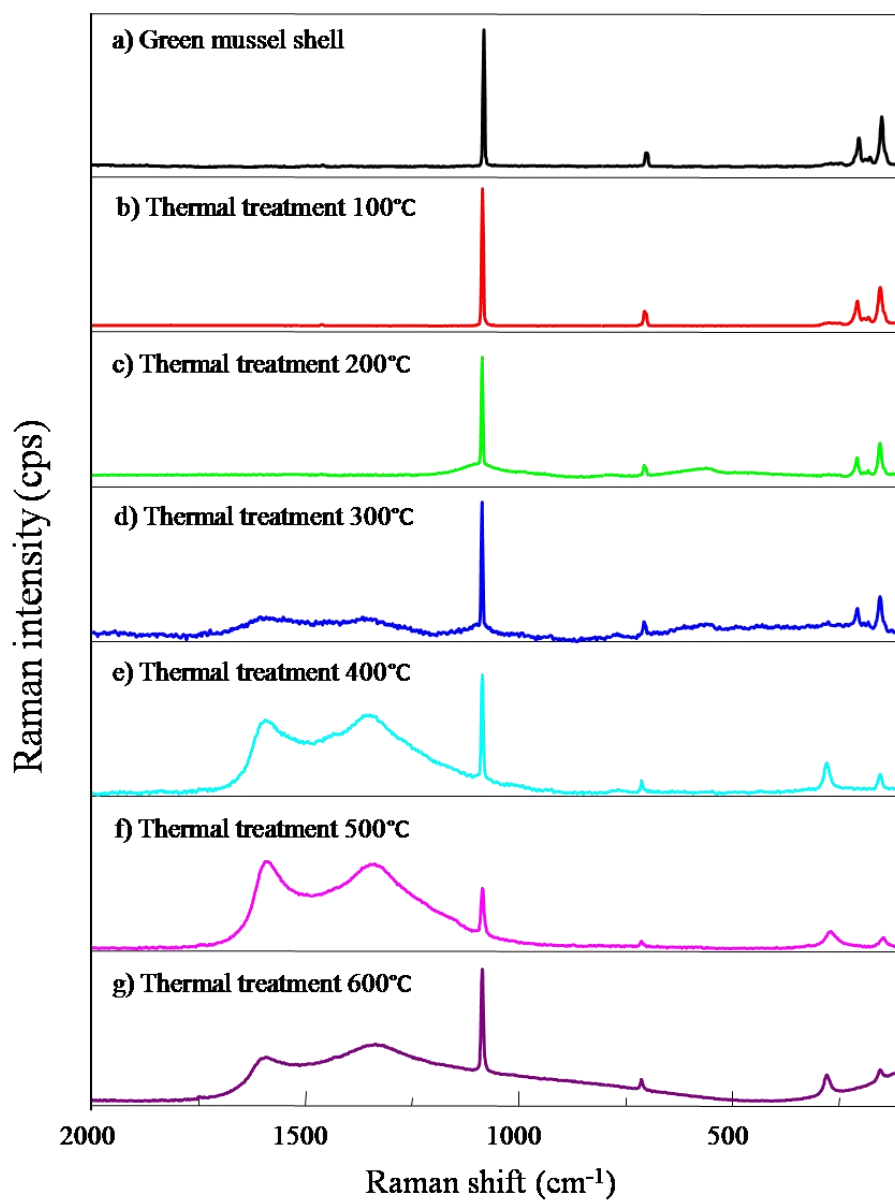
Figure 4.16 Raman spectrum of green mussel shells after calcined at (a) 100 °C, (b) 200 °C, (c) 300 °C, (d) 400 °C, (e) 500 °C, and (f) 600 °C for 2 h, and soaked in 30 wt% H_2O_2 for 24 h.

From Raman spectrum, this method gives the same results as the first method. Moreover, thermal treated at 300 °C was observed D and G bands of carbon specie at 1600 and 1350 cm^{-1} because periostracum was unremoved and burned. It concluded

that thermal treatment eliminated both of periostracum and interlamellar protein at the same time.
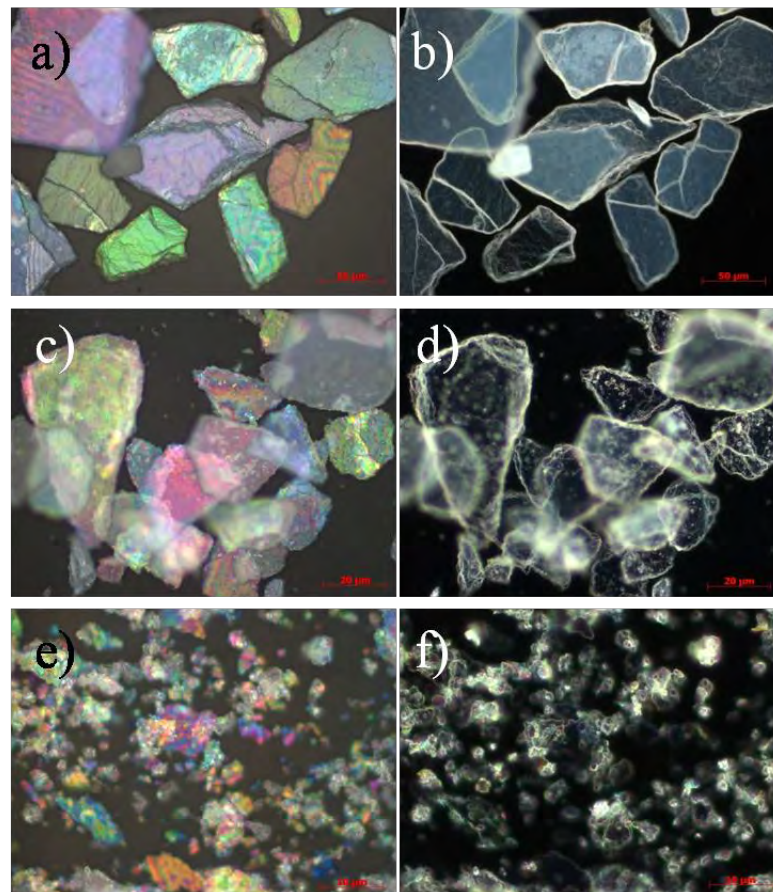
Figure 4.17   Optical microscope images of pearlescent flakes in bright field and dark field mode (a) and b) 200 – 500 μm, (c) and (d) 50 -100 μm, and (e) and (f) 15 – 50 μm.

Pearlescent flakes form this method had less thickness than that from the first method. For example, pearlescent flakes from alkaline and thermal treatment were 50 μm width that thickness is 50 μm, and an aspect ratio (diameter per thickness) of 1:1. Due to, pearlescent flakes from only thermal treatment with the same width (50 μm) the thickness was 5 μm with aspect ratio of 10:1. The developed processes were high quality flakes and reduced cost.
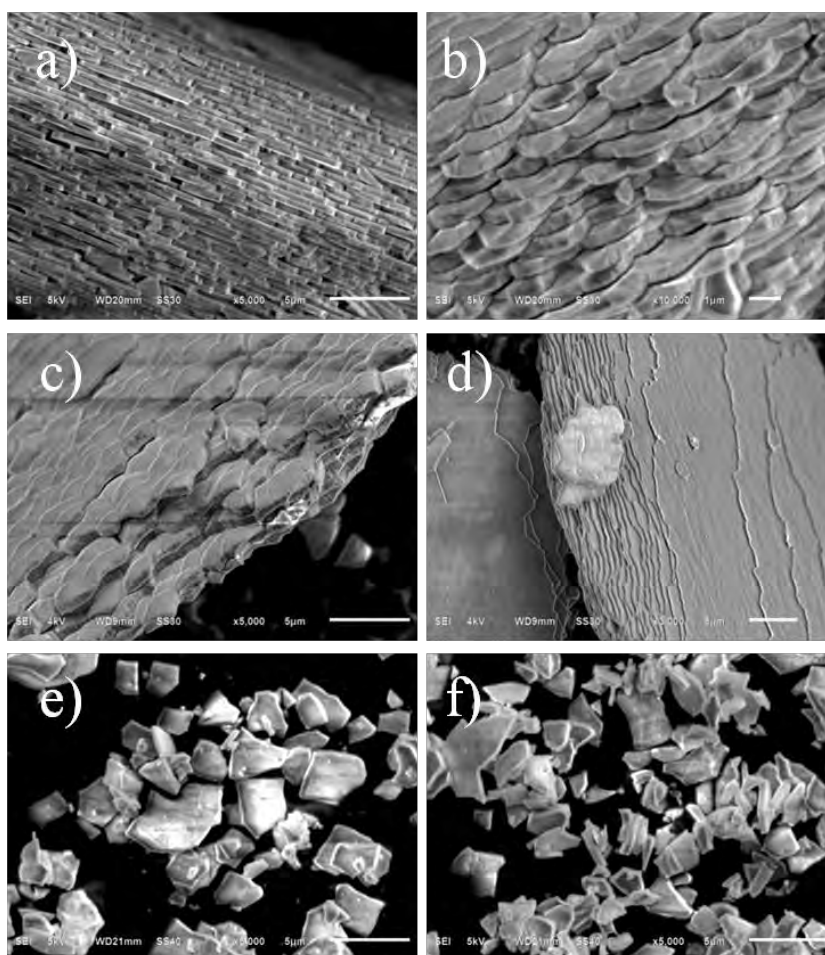
Figure 4.18 SEM images of pearlescent flakes (a) and (b) 200 – 500 µm, (c) and (d) 50 -100 µm, (e) and (f) 15 – 50 µm.

Table 4.4 Advantages and disadvantages between 2 methods.

	Alkaline and thermal treatment	Thermal treatment
Numbers of Steps	4	3
Ease of Washing	Yes	No
Aspect ratio (diameter-to-thick)	1:1	10:1
Sparking	Yes	Yes

4.3 An acidic treatment of pearlescent flakes

The pearlescent flakes form the first method had the problem of smaller calcium carbonate attach to the surface which could not be removed, led to less reflection of light, thus, to fix this problem was to use acidic treatment, 0.5 M HCl, to dissolve the smaller calcium carbonate on the surface.
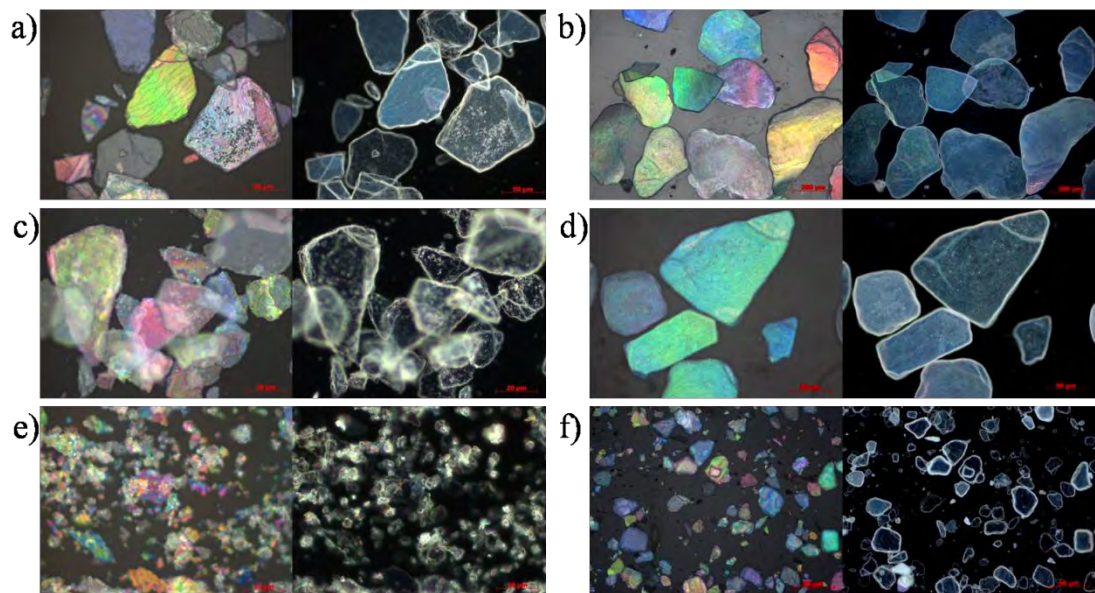
Figure 4.19 Optical microscope images of (a), (c), (e) pearlescent flakes before and (b), (d), (f) after acidic treatment of 200 – 500 μm, 50 -100 μm, and 15 – 50 μm, respectively.

Acidic treated pearlescent flakes surface was cleaner than no treated pearlescent flakes because no smaller calcium carbonate was on the surface, yield in more light reflection and more beautiful.

Table 4.5   Comparisons of pearlescent flakes from green mussel shells and commercial pearlescent pigments (mica).

	Pearlescent flakes from green mussel shell	Pearlescent pigment from mica
Producing processes	Not complicated	Complicated
Machines	Small machines, readily available	Bigger machines, specifically
Prodiction Costs	Low	Hight
Price	Low	High
Sparkling	Yes	Yes

4.4   Application of pearlescent flakes

Pearlescent flakes in the range of 15 – 50 and 50 -100 μm are suitable shimmer for cosmetics, and paint. For example, pearlescent flakes were mixed in cosmetic replaced mica shimmer. (e.g. powder, brush on, and eye shadow)

Figure 4.20 Photographs and optical microscope images of bright field and dark field of (a), (b), and (c) press powder, (e), (f), and (g) brush on, and (h), (i), and (j) eye shadow which were mixed pearlescent flakes from green mussel shell.

CHAPTER V

CONCLUSION

In conclusion, the objective of this research, i.e. preparation of pearlescent flakes from wasted green mussel shell, is achieved. The process included thermal treatment at 200 °C for 2 h, soaked with 30 wt% H_2O_2 solutions for 24 h, washed with deionized water, size selected by mesh, and acidic treatment with diluted hydrochloric acid. The interlamellar protein can be eliminated by thermal and H_2O_2 treatments. Our pearlescent flakes consist of hundreds of aragonite calcium carbonate layers. The aragonite calcium carbonate in each layer is about 5 μm width and 200 – 500 nm thickness with aspect ratio of 10:1. The size of pearlescent flakes can be controlled by the size of the mesh e.g., 15 – 50 μm, 50 – 100 μm, and 200 – 500 μm. The wasted green mussel shells can be obtained by using processes proposed in the research. The pearlescent flakes production is simple, and environmentally friendly. These pearlescent flakes are applicable as shimmers for cosmetics, additives for automotive paints, and decorative items.

From our research we may claim that under the support from the Thai government, this research work will be a part of the contribution in promoting the prosperity of Thai economy parallel to the AEC upcoming protocols.

References

[1]   Appukuttan, K.K. On the occurrence of the green mussel *Perna viridis* (Linnaeus) in Andaman island**.   Indian J. Fish.** 24 (1977) : 244 - 247.

[2]   Amethyst Galleries, Inc. The Mineral CALCITE [Online]. Available from : http://www.galleries.com/Calcite [2013, February 28].

[3]   Amethyst Galleries, Inc. The Mineral ARAGONITE [Online] Available from : http://www.galleries.com/Aragonite [2013, February 28].

[4]   Paula, S.M., and Silveira, M. Studies on molluscan shells: Contributions from microscopic and analytical methods. **Micron.** 40 (2009): 669 – 690.

[5]   Leung, H.M., and Sinha, S.K. Scratch and indentation tests on seashells. **Tribol. Int.** 42 (2009) : 40– 49.

[6]   Liu, Y., and Shigley, J.E. Iridescence color of a shell of the mollusk *Pinctada margaritifera* caused by diffraction. **Opt. Express.** 4 (1999) : 177 – 182.

[7]   Pelesko, J. Wet Edible Pearlescent Film Coatings. **U.S. Patent**, US 2010/0029788 A1, (2010).

[8]   Hollman, A.M., Nicolas, S., Schottland, P., Debacker, M., Antonowicz, A., and Lin, H.H. Multi-Colored Lustrous Pearlescent Pigments. **U.S. Patent**, US 7850755 B2, (2010).

[9]   Hollman, A., Chottland, P., and Black, J. Orange Pearlescent Pigments. **U.S. Patent**, US 2009/0208436 A1, (2009).

[10]   Schweinfurth, R. and Hillgartner, U. Colouring Using Pearlescent Pigments in the Food and Pharmaceutical Sectors. **U.S. Patent**, US 2008/0014321 A1, (2008).

[11]   Melson, S., Entenmann, M., Jekel, M., and Mathias, M. Pearlescent Pigments. **U.S. Patent,** US 2008/0168924 A1, (2008).

[12]   Morita, Y., and Armstrong, J.E. High luster iridescent nacreous pigment. **U.S. Patent** 3,493,410, February 3, (1970).

[13]   Kaupp, G., Schmidt, U., Steinbach, K., and Schumacher, D., Pearlescent Pigments

Containing Cosmetic Compositions. **U.S. Patent**, US 2010/0047300 A1, (2010)

[14]   Meyers, M.A., Lin, A.Y., Chen, P., and Muyco, J. Mechanical strength of abalone nacre: Role of the soft organic layer. **J. Mech. Behav. Biomed.** 1 (2008) **:** 76 − 85.

[15]   Meyers, M.A., Chen, P.Y., Lopez, M.I., Seki, Y., and Lin, A.Y.M. Biological materials: A materials science approach. **J. Mech. Behav. Biomed.** 4 (2011) : 626 − 657.

[16]   Ballarini, R., and Heuer, A.H. The body armor of the queen conch is much tougher than comparable synthetic materials. What secrets does it hold?. **Am. Sci.** 95 (2007) **:** 422 − 429.

[17]   Dauphin, Y., and Denis, A. Structure and composition of the aragonitic crossed lamellar layers in six species of Bivalvia and Gastropoda. **Comp. Biochem. Physiol. A** 126 (2000) : 367 − 377.

[18]   Rousseau, M., Lopez, E., Couté, A., Mascarel, G., Smith, D.C., Naslain, R., and Bourrat, X. Sheet nacre growth mechanism: a Voronoi model. **J. Struct. Biol.** 149 (2005) : 149–157.

[19]   Rousseaua, M., Lopez, E., Stempfle, P., Brendle, M., Franke, L., Guette, A., Naslaind, R., and Bourrat, X. Multiscale structure of sheet nacre. **Biomaterials** 26 (2005) : 6254–6262.

[20]   Xie, L., Wang, X.X., and Li, J. The SEM and TEM study on the laminated structure of individual aragonitic nacre tablet in freshwater bivalve *H. cumingii Lea* shell. **J. Struct. Biol.** 169 (2010) : 89–94.

[21]   Al-Barwani, S.M., Arshad, A., Nurul Amin, S.M., Japar, S.B., Siraj, S.S., and Yap, C.K. Population dynamics of the green mussel *Perna viridis* from the high spat-fall coastal water of Malacca, Peninsular Malaysia. **Fish. Res.** 84 (2007) : 147–152.

[22]   Cheung, S.G. Population dynamics and energy budgets of green-lipped mussel *Perna viridis* (Linnaeus) in a polluted harbour . **J. Exp. Mar.**

Biol. Ecok. 168 (1993) : 1-24.

[23] Laxmilatha, P., Rao, G.S., Patnaik, P., Rao, T.N., Rao, M.P., and Dash, B. Potential for the hatchery production of spat of the green mussel *Perna viridis* Linnaeus (1758). **Aquaculture** 312 (2011) : 88–94.

[24] Rajagopal, S., Venugopalan, V.P., van der Velde, G., and Jenner, H.A. Greening of the coasts: a review of the *Perna viridis* success story. **Aquat. Ecol.** 40 (2006) : 273-297.

[25] Shin, P.K.S., Yau, F.N., Chow, S.H., Tai, K.K., and Cheung, S.G. Responses of the green-lipped mussel *Perna viridis (L.)* to suspended solids. **Mar. Pollut. Bull.** 45 (2002) : 157–162.

[26] Boonyatumanond, R., Jaksakul, A., Puncharoen, P., and Tabucanon , M.S. Monitoring of organochlorine pesticides residues in green mussels (*Perna viridis*) from the coastal area of Thailand. **Environ. Pollut**. 119 (2002) : 245–252.

[27] Wu, R.S.S., and Lam, P. K.S. Glucose-6-Phosphate Dehydrogenase and Lactate Dehydrogenase in the Green-lipped mussel (*Perna viridis*): Possible Biomarkers for Hypoxia in the Marine Environment. **War. Res**. 31 (1997) : 2797 - 2801.

[28] Cheung, S.G. and Cheung , R.Y.H. Effects of Heavy Metals on Oxygen Consumption and Ammonia Excretion in Green-Lipped Mussels (*Perna viridis*). **Mar. Pollut. Bull.** 31 (1995) : 381-386.

[29] Krishnakumar, P.K., Asokan, P.K., and Pillai, V.K. Physiological and cellular responses to copper and mercury in the green mussel *Perna viridis* (Linnaeus). **Aquat. Toxicol.** 18 (1990) : 163-174.

[30] D'Silva, C. and Kureishy, T.W. Experimental Studies on the Accumulation of Copper and Zinc in the Green Mussel. **Mar. Pollut. Bull.** 9 (1987) : 187-l90.

[31] Harino, H., Ohji, M., Wattayakorn, G., Arai, T., Rungsupa, S., and Miyazaki, N. Occurrence of Antifouling Biocides in Sediment and Green Mussels from

Thailand. **Arch. Environ. Contam. Toxicol.** 51 (2006) : 400–407.

[32] Menasveta, P. and Cheevaparanapiwat, V. Heavy Metals, Organochlorine Pesticides and PCBs in Green Mussels, Mullets and Sediments of River Mouths in Thailand. **Mar. Pollut. Bull.** 12 (1981) : 19-25.

[33] Holmesl, M.J., Teo, S.L.M., Lee, F.C., and Khoo, H.W. Persistent low concentrations of diarrhetic shellfish toxins in green mussels *Perna viridis* from the Johor Strait, Singapore: first record of diarrhetic shellfish toxins from South-East Asia. **Mar. Ecol. Prog. Ser.** 181 (1999) : 257-268.

[34] Experimental Biosciences. **Dark Field Viewing** [Online]. Available from : http://www.ruf.rice.edu [2013, February 28].

[35] Fuller, M.P., and Griffiths, P. R. Diffuse Reflectance Measurements by Infrared Fourier Transform Spectrometry. **Anal. Chem.** 50 (1978) : 1906 – 1910.

[36] Cartwright, J.H.E. and Checa, A.G. The dynamics of nacre self-assembly. **J. R. Soc. Interface.** 4 (2007) : 491–504.

[37] Hongyan, M., Beili, Z., Zuolu, Q., Zhangfa, T., and Shuheng, Q. Aragonite observed in the prismatic layer of seawater-cultured pearls. **Front. Mater. Sci. China** 1 (2007) : 326 – 329.

[38] Bezares, J., Asaro, R.J., and Hawley, M. Macromolecular structure of the organic framework of nacre in *Haliotis rufescens*: Implications for growth and mechanical behavior. **J .Struct. Biol.** 163 (2008) : 61 – 75.

[39] Verma, D., Katti, K., and Katti, D. Photoacoustic FT-IR spectroscopic study of undisturbed nacre from red abalone. **Spectrochim. Acta. A.** 64 (2006) : 1051–1057.

[40] Zhong, C. and Chu, C.C. On the Origin of Amorphous Cores in Biomimetic $CaCO_3$ Spherulites: New Insights into Spherulitic Crystallization. **Cryst. Growth. Des.** 10 (2010) : 5043 – 5049.

[41] Alia, J.M., de Mera, Y.D., Edwards, H.G.M., Martin, P.G., and Andes, S.L. FT-Raman and infrared spectroscopic study of aragonite-strontianite $(Ca_xSr_{1-x}CO_3)$ solid solution. **Spectrochim. Acta. A.** 53 (1997) : 2347-2362.

[42]   Wang, R.Z., Suo, Z., Evans, A.G., Yao, N., and Aksay, I.A. Deformation
          mechanisms in nacre. **J. Mater. Res**. 16 (2001) : 2485 – 2493.

[43]   Yan, Z., Fang, Z., Ma, Z., Deng, J., Li, S., Xie, L., and Zhang, R.
          Biomineralization: Functions of calmodulin-like protein in the shell formation
          of pearl oyster. **Biochim. Biophys. Acta.** 1770 (2007) : 1338–1344**.**

[44]   Malvern Instruments Ltd. Sample dispersion & refractive index guide. 3.1.
          Worcestershire: Malvern Instruments Ltd. 1997.

[45]   Hook, F., Voros, J., Rodahl, M., Kurrat, R., Boni, P., Ramsden, J.J., Textor, M.,
          Spencer, N.D., Tengvall, P., Gold, J., and Kasemo, B. A comparative study of
          protein adsorption on titanium oxide surfaces using in situ ellipsometry,
          optical waveguide lightmode spectroscopy, and quartz crystal
          microbalance/dissipation. **Colloid. Surface. B**. 24 (2002) : 155–170.

[46]   Marchon, B., Gui, J., Grannen, K., and Rauch, G.C. Photoluminescence And
          Raman Spectroscopy in Hydrogenated Carbon Film. **IEEE T. Magn**. 33
          (1997) : 3148 – 3150.

VITAE

Name:　　Miss Thiluksakorn Jirapisitkul

Date of Birth:　November 17, 1988　　**Birth place:**　Samut Songkram
Province, Thailand

Address:　7/25 Soi Phahonyothin 24, Yaek 2-1-2, Chompon, Jatujak,
Bangkok, Thailand 10240
E-mail address: t.jirapisitkul@gmail.com

Education:

2011　　Bachelor of Science (Chemistry, 2nd Class Hons), Chulalongkorn
University, Bangkok, Thailand

2013　　Master of Science (Chemistry), Chulalongkorn University,
Bangkok, Thailand

Conferences and Awards:

March, 2011　The Hitachi Trophy 2011 (The 19th Annual Academic Meeting of
the Faculty of Science, Chulalongkorn University)
2nd Prize Award

January, 2012　The 29th Annual Conference of The Microscopy Society of
Thailand, Cha-am, Thailand

March, 2012　The Science Forum 2012 (The 20th Annual Academic Meeting of
the Faculty of Science, Chulalongkorn University)

January, 2013　The 30th Annual Conference of The Microscopy Society of
Thailand, Chanthaburi, Thailand